

Strain stiffening universality in composite hydrogels and tissues

Jake Song,^{1,2,#,*} Elad Deiss-Yehiely,^{1,3} Serra Yesilata,² and Gareth H. McKinley^{2,*}

¹Department of Materials Science and Engineering, Massachusetts Institute of Technology

²Department of Mechanical Engineering, Massachusetts Institute of Technology

³Koch Institute for Integrative Cancer Research, Massachusetts Institute of Technology

[#]Department of Mechanical Engineering, Stanford University

*Correspondence to jakesong@stanford.edu, gareth@mit.edu

Soft biological tissues exhibit a remarkable resilience to large mechanical loads, a property which is associated with the strain stiffening capability of the biopolymer networks that structurally support the tissues.^{1,2} Yet, recent studies have shown that composite systems such as tissues and blood clots exhibit mechanical properties that contradict those of the polymer matrix – demonstrating stiffening in compression, but softening in shear and tension.³ The microscopic basis of this apparent paradox remains poorly understood. We show that composite hydrogels and tissues do indeed exhibit non-linear elastic stiffening in shear – which is governed by the stretching of the polymer chains in the matrix – and that it is driven by the same mechanism that drives compression stiffening. However, we show that the non-linear elastic stiffening in composite hydrogels and tissues is masked by mechanical dissipation arising from filler-polymer interactions known as the Mullins effect,⁴ and we introduce a method to characterize the non-linear elasticity of the composites in isolation from this overall strain softening response through large-amplitude oscillatory shear experiments.⁵ We present a comprehensive characterization of the non-linear elastic strain stiffening of composite hydrogels and soft tissues, and show that the strain stiffening in shear and compression are both governed by universal strain amplification factors that depend on essential properties of the composite system, such as the filler concentration ϕ and the filler-polymer interaction strength ε . These results elucidate the microscopic mechanisms governing the non-linear mechanics of tissues, which provides design principles for engineering tissue-mimetic soft materials, and have broad implications for cell-matrix mechanotransduction in living tissues.⁶⁻⁸

We first demonstrate the compression stiffening of a filled composite hydrogel consisting of Ca^{2+} -crosslinked pectin and dextran particles, with systematically varied particle volume fraction ϕ and two different particle-polymer interaction strengths ε (Fig. 1A). The particles are large (diameter of $\sim 120 \mu\text{m}$, Fig. S1), and can sediment readily before gelation occurs; we address this by adding Carbopol into the hydrogel, which prevents sedimentation through yield stress stabilization of the particles (Fig. S2). We perform quasi-static compression experiments on the composite hydrogels (Fig. 1B); our systems are completely compressible under these conditions, as revealed by an analysis of the Poisson's ratio ν during compression (Fig. S4). The experiments show that the pectin hydrogels undergo an increase in the linear shear modulus with increasing ϕ , and also exhibit greater non-linear stiffening in $G'(\lambda)$, the storage modulus as a function of axial strain λ (Fig. S5A). This compression stiffening effect is amplified in composite hydrogels with

higher ε , as hydrogels with positively charged cationic (C) particles exhibit greater compression stiffening compared to neutral (N) particles (Fig. S5B), an effect which is independent of both the filler concentration and the linear modulus of the hydrogel (Fig. S5C). We find that the normalized compression stiffening curves as a function of ϕ and ε can be shifted onto a universal master curve (Fig. 1C), with the associated compressive strain amplification factor a_λ systematically increasing with ϕ and ε (Fig. 1D).

There are two recent models to rationalize the observed compression stiffening in the composite hydrogels. One is the numerical models of van Oosten et al., which show that volume-conserving fillers can cause amplified stretching of the polymers under compression by restricting interstitial space.³ The other is the simulation result of Shivers et al., which show that compression causes deformation of rigid fillers, which then causes stretching of the bonded polymers in a percolated filler-polymer network, and eventually jamming of the fillers themselves.⁹ We find that our results are more consistent with those of Shivers et al., as we observe clearly demarcated regimes of bending, stretching, and jamming in our master curve that are predicted in simulations (Fig. 1C), which is absent in the numerical models of van Oosten et al.

The agreement with the simulation predictions of Shivers et al., provides an appropriate context to understand the higher compressive strain amplification factor a_λ observed in composite hydrogels with higher ε . The onset of the steep increase in $G'(\lambda)$ at low λ and the reduction in slope at high λ can be attributed to compression-induced structural transitions of the fillers – percolation and jamming, respectively. While the percolation threshold is difficult to isolate in the system as the polymer network alone exhibits stiffening at large λ , the jamming threshold can be isolated from the curve as occurring approximately at $\lambda_{jam} = 1.25/a_\lambda$ (Fig. 1C). A systematic evaluation of this knee point over two sets of experiments allows us to characterize the particle jamming threshold $\phi_{jam} = \phi/(1 - \lambda_{jam})$, yielding $\phi_{jam}(C) = 0.49$ and $\phi_{jam}(N) = 0.82$ (Fig. S7). Given the same size and stiffness of the particles, we interpret this difference in ϕ_{jam} as arising from the larger effective volume ϕ_{eff} (and effective radius r_{eff}) of the more attractive C particles relative to the N particles. The relative r_{eff} of the C particles relative to the N particles, χ , can be calculated via the relation $\chi = r_{eff}(C)/r_{eff}(N) = (\phi_{jam}(N)/\phi_{jam}(C))^{1/3} = 1.18$, which suggests that the hydrogels with C particles effectively contain fillers that have 18% greater effective radii than those with N particles.

These findings are corroborated by comparing the linear shear modulus of the hydrogels at zero axial strain $G'(0)$, which are systematically higher for hydrogels with C fillers than N fillers at all ϕ . We find the filler-induced reinforcement effect in our hydrogels to be substantially greater than that expected from the phantom network theory.¹⁰ We thus fit the results to a more classical reinforcement model of the form:

$$G'(0)/G'_{pec}(0) = 1 + 2.5\phi_{eff} + c_2\phi_{eff} \quad (1)$$

where c_2 is the second virial coefficient which can vary from 2.5 to 15.6,¹¹ and $\phi_{eff} = (r_{eff}/r)^3\phi$. This model is often referred to as the hydrodynamic model as it is analogous to the solution for the hydrodynamic interactions in suspensions,¹² and it carries limitations that prevent

a rigorous measure of r_{eff} for our purposes, such as the neglecting of multi-body particle interactions at high ϕ , and the effects of using different values of c_2 on the obtained r_{eff} . Despite these shortcomings, we still find that the model provides insight into the relative difference in r_{eff} of the C and N filled systems, which we find to be $\chi = 1.16$ using $c_2 = 14.1$ by Guth and Gold (Fig. 1E),¹³ and $\chi = 1.17$ using $c_2 = 5.2$ by Batchelor and Green (Fig. S8),¹⁴ both of which are in excellent agreement with $\chi = 1.18$ obtained from the jamming threshold measurements. Together, these results suggest that strong filler-polymer interactions ε can increase the effective size of the particles by forming a larger layer of densified and immobile polymers on the particle surface (Fig. 1F), consistent with what is understood about interphase formation in polymers composites.^{15,16} Interestingly, the compressive strain amplification factor a_λ shows a collapse when plotted as a function of $\chi^3 \phi$ (Fig. 1D), where χ is the effective radius of the C fillers relative to the N fillers (i.e., $\chi(C) = 1.16$, $\chi(N) = 1$). This shows that a difference in ϕ_{eff} can adequately explain the strain amplification observed in composite hydrogels with different filler-polymer interaction strength ε .

Composite hydrogels and tissues have been shown to exhibit strain softening in tension and shear, in contrast to the stiffening observed in compression shown thus far.^{3,17} This behavior appears paradoxical given the dramatic tension and shear stiffening exhibited by their constituent biopolymers matrix.^{1,2} The aforementioned lattice-based numerical model³ rationalizes this tension softening in composite hydrogels through a mechanism by which volume-conserving fillers shield the polymer matrix from strain. More generally however, this form of tension and shear strain softening effect has been observed in polymeric composites for many decades, and is canonically described as the Payne effect¹⁸ (in which the storage modulus G' decreases with increasing strain amplitude γ_0 , and in which the loss modulus G'' exhibits an overshoot at the yield point) and the Mullins effect⁴ (in which stress softening occurs with increasing cyclic strain), depending on the experimental protocol. Consistent with these past observations, we observe strain softening in composite hydrogels under large-amplitude oscillatory shear (LAOS); while pectin hydrogels exhibit strain stiffening, evidenced by an increase in G' with increasing γ_0 , hydrogels filled with C and N particles do not exhibit any form of stiffening in shear (Fig. 2A). However, since the raw stress waveform becomes distorted in LAOS experiments, the G' and G'' computed by the rheometer (which consider just the first-harmonic response of the stress and strain, and are denoted G'_1 and G''_1) provide an oversimplified description of the non-linear mechanics of both systems (Fig. 2B,C).¹⁹ An alternative method of analysis is clearly needed to extract non-linear elasticity in these systems.

One known method is to compute the differential storage modulus at the maximum strain of each cycle, $G'_K(\gamma_0) = (d\sigma'/d\gamma)|_{\gamma_0}$, where σ' is the elastic component of the total stress (Fig. 2B).²⁰ This quantity is the LAOS-equivalent of the differential storage modulus $K'(\sigma_0)$ obtained by superimposing a small-amplitude oscillatory shear on a step stress σ_0 , frequently used to characterize the non-linear elasticity of biopolymer networks.^{21,22} Analysis of $G'_K(\gamma_0)$ for our systems reveals shear strain stiffening in the composite hydrogels, but at a lower magnitude compared to the pectin hydrogels (Fig. S9A). The raw stress-strain Lissajous curves of the pectin hydrogels and composite hydrogels provide clues on why composite hydrogels exhibit lower

$G'_K(\gamma_0)$ than pectin hydrogels: while the $\sigma'(t)$ curves of the pectin hydrogels are superposed on each other at all γ_0 until reaching the yield strain (the point of significant decrease in G'_1 with γ_0 , Fig. 2A), the $\sigma'(t)$ curves of the composite hydrogels are horizontally translated at γ_0 much below the yield strain (Fig. 2B,C). These results show that inelastic dissipation occurs prominently in the composite hydrogels prior to yielding, thus obfuscating measurements of non-linear elasticity in these systems.

These inelastic effects can be attributed to elastoplastic deformations that occur in the gels prior to macroscopic yielding. Evidence for these effects can be seen in the offshoot in the G'' in the composite hydrogels prior to yielding, which is a hallmark property of the Payne effect¹⁸ and a measure of the irrecoverable plastic deformation that occurs in the microstructure in the non-linear regime.²³ Further evidence for these effects are revealed by cyclic compression and transient LAOS experiments on the composite hydrogels, which show that subsequent loading curves memorize and trace the previous unloading curves, with increasing plasticity per loading cycle (Fig. S10) – a hallmark property of the Mullins effect.⁴ The Mullins effect therefore leads to a horizontal translation of $\sigma'(t)$ (Fig. S10F), and a softening effect that is convolved in measurements of G'_1 (Fig. 2A) and $G'_K(\gamma_0)$ (Fig. S10). In the absence of such elastoplastic effects, we may expect the non-linear elasticity of the pectin hydrogels and composite hydrogels to be coincident. This would correspond to the physical scenario predicted by Shivers et al., in which plastic effects are absent (as polymers are permanently bound to the particles), and in which tension causes stiffening via stretching of the bridging polymers.⁹

We show that the Mullins effect observed in LAOS (Fig. 2C, Fig. S10) can be eliminated to obtain the true non-linear elastic response of the system by computing the *strain-dependent differential storage modulus*, $G'_K(\gamma) = d\sigma'/d\gamma$ (Fig. 2C inset). The $G'_K(\gamma)$ curves as a function of the input oscillation amplitude γ_0 for the pectin and composite hydrogels are self-similar, but the latter results become horizontally off-set with increasing γ_0 due to the Mullins effect (Fig. 2D,E). The translated $G'_K(\gamma)$ curves can thus be shifted onto a reference $G'_K(\gamma)$ curve in the linear regime to construct a master curve for each system, via the Mullins shift factor M_f which then provides a quantitative measure of γ_0 -dependent elastoplasticity in the system. The M_f values are near unity for the pectin hydrogels at all γ_0 (minimal elastoplastic effects), and increases in composite hydrogels with increasing ϕ and ε (Fig. 2F). The observation of greater M_f in attractive hydrogels with C particles compared to N particles is also supported by the differences in the Mullins effect observed in cyclic compression experiments for these two systems (Fig. S10B-E). Overall, these results suggest that stronger filler-polymer interaction strength ε result in greater elastoplastic effects in composite hydrogels. This can be rationalized by the greater degree of immobilization of the polymers on the particle surface with increasing ε (Fig. 1F),^{15,16} as the Mullins and Payne effects can be attributed to the strain-induced breakage of the immobilized polymers on the particle surface which bridge the particles,^{24,25} It is noted that the M_f data for composite hydrogels with N particles are truncated at higher γ_0 due to the system exhibiting clear signatures of slip before yielding occurs, namely a gradual drop in G'_1 and G''_1 prior to yielding (Fig. 2A, S12A)²⁶ and a softened response in the $G'_K(\gamma)$ curve which results in deviations from the reference curve (Fig.

S12B,G). We find neither the pectin hydrogels nor the composite hydrogels with C fillers affected by these artifacts during measurement.

The M_f -shifted $G'_K(\gamma)$ curves provide an unadulterated characterization of the non-linear elasticity of composite systems (Fig. S13A). The M_f -shifted $G'_K(\gamma)$ curves for pectin and composite hydrogels are self-similar, and can be shifted onto a single master curve using a shear strain amplification factor a_γ – in similar vein as the results from compression experiments (Fig. S13B). In fact, we find that both the compression and shear stiffening of composite hydrogels as a function of ϕ and ε can be described by a universal master curve (Fig. 2G), with coincident values of a_λ and a_γ (Fig. 2H). These results demonstrate the universal non-linear elastic response of composite hydrogels in compression and shear, which is governed by the stretching of the matrix polymer chains – in broad agreement with the simulation results of Shivers et al., who observe a similar universality in compression and tension (in the absence of plasticity).⁹ These results also demonstrate the critical roles played by ϕ and ε – which are fundamental parameters in biological tissues – in amplifying the non-linear mechanical responses of the system.

The exact mechanism underlying the ϕ and ε induced strain amplification in composite hydrogels remains unexplored. Shivers et al.,⁹ suggest that this amplification is correlated by an increase in the non-affine deformation of fillers that arises at high ϕ . While such non-affine deformations are likely prevalent in composite hydrogels,^{27,28} their causational role in amplifying the stretching response of the polymer matrix is not established. As a counter-example to this idea, we find that the strain amplification factors a_λ and a_γ can be reasonably described, parameter-free, by a simple 1-D filler-induced affine strain amplification model (Fig. 2I)²⁹:

$$a_i / a_i(0) = 1 / (1 - \phi^{1/3}) \quad (2)$$

where $i = \lambda$ or γ . The remarkable simplicity of this description is rather appealing; however since there is still a lack of consensus on the exact functional form to describe strain amplification in composite systems,¹¹ an independent verification through molecular-scale investigation would be an important next step.

It is also interesting to compare strain amplification with the increase in elastic modulus with filler loading. We find that a_λ and a_γ roughly trace the linear shear modulus G'/G'_0 at $\phi \leq 0.2$, suggesting that strain amplification can provide an empirical description of the increased elasticity of composite systems at low filler concentrations (Fig. S15), even if it does not account for some of the pertinent physics arising from filler incorporation such as the hydrodynamic reinforcement effect.^{11,30,31} However, we find that G'/G'_0 exhibits a steep increase, and deviates from a_λ and a_γ at $\phi > 0.2$ (Fig. S15). This steep increase in G'/G'_0 can be explained by the emergent elasticity of a percolated particle-polymer network,^{16,25,32,33} the presence of which is evidenced in the hallmark behaviors of our composite hydrogels such as compression stiffening,⁹ and elastoplastic dissipation at large γ_0 .²⁴

Our experimental results and the simulation results of Shivers et al.⁹ demonstrate a strain stiffening universality in composite hydrogels where stiffening is equally amplified in shear and in compression by parameters such as ϕ and ε . However, both systems demonstrate this effect on

model composite hydrogels which are structurally different to tissues. The model of Shivers et al. utilize fiber networks with rigid inclusions, while our system utilizes polysaccharides also with relatively stiff inclusions ($\sim 10^6$ Pa).³⁴ These model systems are not equivalent to soft tissues which are multi-polymer composites of flexible proteoglycans and fibrous polymers embedded with *cells*, which have a low stiffness ranging from $10^2 \sim 10^5$ Pa,³⁵ and which exhibit matrix-stiffening contractile activity.³⁶ Thus, the broad implications of strain stiffening universality remains unclear in soft biological tissues, especially in shear where mostly softening responses have been observed thus far^{3,17}.

To explore this, we perform compression stiffening experiments on mouse tissues: lung, heart, adipose, liver, and partially-decellularized (PD) liver (Fig. 3A, S16). We find the tissue samples to be less compressible than the composite hydrogels, with ν ranging from 0.2 to 0.4, which is indicative of their low poroelasticity relative to the hydrogels (Fig. S17).³⁷ All moduli data can be superposed onto the lung data which shows the weakest compression stiffening (Fig. 3B). The first harmonic G'_1 collected from LAOS experiments on the tissues show an even more pronounced Payne effect (Fig. 3C) compared to the composite hydrogels (Fig. 2A), and correspondingly, the Lissajous curves exhibit substantial horizontal translation (Fig. 3D). The Lissajous curves also show significant strain-stiffening behavior in $\sigma'(t)$, which we can now extract via our $G'_K(\gamma)$ protocol.

To our knowledge, this represents the first isolated characterization of the non-linear elasticity of biological tissues. As such, we first analyze $G'_K(\gamma)$ as a function of elastic stress σ' , from which we can gain molecular insights into the origin of non-linear elasticity in tissues. There is extensive literature on the origins of the scaling of the differential modulus with stress, i.e. $G'_K(\gamma) \sim \sigma'^z$, which is most commonly assumed to arise due to the force-displacement response of the individual polymer strands.^{2,21,38} In this case, z should follow the force-extension (F-L) relationship of individual polymer or filament strands (which can be characterized by atomic force microscopy experiments), with $dF/dL \sim F^z$.²¹ The most common value of z is the case when polymers follow entropic elasticity predicted by the worm-like chain (WLC) model,³⁹ in which case $z = 1.5$, though this number can be lower in biopolymers which are more extensible or have enthalpic components to the elasticity. Pectin, like other polysaccharides,⁴⁰ exhibits a more extensible force-extension relationship of $dF/dL \sim F^{1.1}$ (Fig. S18A),⁴¹ and we indeed also observe that $G'_K(\gamma) \sim \sigma'^{1.1}$ in our systems (Fig. S18B). This shows that polymer chain stretching underlies the non-linear elasticity of pectin hydrogel and the composites; a similar mechanism might be responsible for the $z < 1.5$ scaling of the differential modulus observed in other polysaccharide gels in literature, for example agarose⁴² and chitosan.⁴³

As for tissues, we may expect tissues to exhibit a scaling of $G'_K(\gamma) \sim \sigma'^{1.5}$ as a host of biopolymers that are constituted in tissues follow the WLC model, such as actin,⁴⁴ collagen molecules,⁴⁵ and proteoglycans.⁴⁶ On the other hand, tissue mechanics are often assumed to be dominated by the collagen fiber network in the connective tissue extracellular matrix (ECM) scaffold. Collagen fibers are hierarchical assemblies of collagen molecules, have persistence lengths on the order of cm,⁴⁷ and do not follow WLC behavior.⁴⁸ Reconstituted collagen fiber networks show a scaling of $z < 1.5$ in the differential modulus, and are often interpreted to arise

from the stress stabilization of subisostatic networks.^{49,50} We find that all our tissues – both whole organs and the connective tissue adipose – follow a scaling of $G'_K(\gamma) \sim \sigma'^{1.5}$ (Fig. 3E). This suggests that non-linear shear strain induces stretching of polymer chains and filaments in the tissues, rather than directly engaging the non-linear response of the collagen fiber network in the ECM. Prior studies show in tension experiments on rat tendon that the total strain of the whole tendon is greater than those experienced by the collagen fibers inside the tendon, thus suggesting that the strain primarily occurs in the proteoglycan-rich matrix.^{48,51} Our results reinforce this observation, and show that this phenomenon may apply generally to organs and connective tissues. The observation of $G'_K(\gamma) \sim \sigma'^{1.5}$ also allows us to rule out the effect of slip in determining the non-linear elasticity of tissues, as the obtained $z = 1.5$ is the upper limit of the theoretical expectations and slip would cause a reduction in z (Fig. S12B,G).

We now return to the γ -dependence of $G'_K(\gamma)$ in tissues. As hinted by the significant Payne effect (Fig. 3C) and the horizontal translation of the Lissajous curves with γ_0 (Fig. 3D), the Mullins factors M_f of the tissue samples are noticeably higher than that observed in the composite hydrogels (Fig. 3F, S21B). We also find that M_f is reasonably self-similar across different tissues, and that the trend is not necessarily correlated to an earlier onset of strain stiffening (evidenced by the lung exhibiting the greatest M_f). This result suggests the presence of dissipative mechanisms other than those governing our composite hydrogel system. An example of such a mechanism would be the scission of covalent bonds in the interpenetrating biopolymer networks in the ECMs,⁵² which could be replicated using a composite hydrogel system with interpenetrating polymer networks. The different onset strain for non-linear elastic stiffening appear to agree with that observed in compression (Fig. S20A), and indeed, the data can also be shifted onto a master curve with the shear strain amplification factor a_γ (Fig. S20B). Thus, similar to that observed in composite hydrogels (Fig. 2G), we observe a universal master curve for various tissues as a function of compression and shear (Fig. 3G). Furthermore, we observe that the strain amplification factors a_λ and a_γ (shifted with reference to the lung data) are practically equivalent for all tissues, and that they also deviate from $G'(0)/G'_{lung}(0)$ (Fig. 3H).

In total, these results demonstrate strain stiffening universality in tissues, which shows that a universal strain amplification mechanism – distinct from that which governs linear elasticity – governs the non-linear mechanics tissues in shear and in compression. The observation of this effect in tissues (Fig. 3G) and in composite hydrogels (Fig. 2G) confirms the idea that tissue mechanics can be modeled by a composite hydrogel consisting of strain-stiffening polymers and attractive fillers.^{3,9} This in turn suggests that key variables that govern composite hydrogel mechanics, such as ϕ and ε , can play an important role in the non-linear mechanics of tissues. In tissues, this implies that cell density as well as cell-matrix adhesion strength can amplify, and thus cause an earlier onset of, the non-linear mechanical response of tissues which is dictated by chain stretching. These results also imply that cell-matrix interactions can cause a densification of polymers in the vicinity of cells, which is indeed observed in studies of cells and fibrous ECM polymers,^{53,54} and that such densification can influence the non-linear mechanics of the system.

The molecular mechanisms underlying the observed strain amplification in composite hydrogels is an important subject for future work that would provide a better understanding of the non-linear mechanics of tissues. Beyond this, tissues also exhibit additional complexities not found in composite hydrogels that could contribute to non-linear mechanics, such as directional alignment of the ECM due to contractile activity^{36,53-55}, softness of the cells,³⁵ interpenetrating biopolymers in the ECM,⁵⁶ and cell-cell aggregations in the development of epithelial tissues and tumors. Deciphering the roles played by these different mechanisms on the non-linear response of tissues could provide important insights into the mechanotransduction pathways of development⁷ and disease,^{8,57} and offer rigorous guidance on designing tissue-mimetic soft materials.

Acknowledgement

J.S. acknowledges financial support from the MIT Lemelson-Vest award and the MIT MathWorks fellowship. J.S. and G.H.M acknowledge helpful discussions with I. Dellatolas (MIT), I. Bischofberger (MIT), E. Del Gado (Georgetown), and J. Shivers (U Chicago).

Methods

Composite hydrogel. The hydrogels were prepared using similar protocol reported for alginate⁵⁸, by mixing aqueous solutions of low-methoxy pectin (Unipectin 700, Cargill) with CaCO_3 at a stoichiometric ratio of 1 Ca^{2+} : 2 COO^- present in the galacturonic acid groups. Carbopol (940, Lubrizol) and dextran particles (Sephadex A-25 and G-25, Cytiva) were then added to the system, and lastly glucono-D-lactone (GDL) was added at a stoichiometric ratio of 1 Ca^{2+} : 3 GDL to induce Ca^{2+} dissolution and gelation. The composite hydrogels had a final composition of 1 wt. % pectin, 0.5 wt. % Carbopol (see flow curve in Fig. S2), and varying wt. % of dextran to meet target volume fraction of their swollen state ϕ (see details in Fig. S1).

Tissues. All animal experiments were approved by the Massachusetts Institute of Technology Committee on Animal care protocol 0720-048-23. Tissues were collected from 20 week old outbred CD-1 mice (Charles River Laboratory) that were euthanized by CO_2 asphyxiation and confirmed via a cervical dislocation. Lung, heart, liver, and omentum adipose were collected from the mice, stored in PBS solution on top of ice, and analyzed within six hours of euthanasia (sample pictures in Fig. S16). Partially decellularized (PD) liver were prepared by immersing a liver sample in 2 % Triton-X solution for 24 hours, following adaptations of literature protocol³.

Rheology. Compression and shear experiments were conducted using the Anton Paar MCR-302 and the TA DHR-3 rheometer. Compression experiments were done by performing a $\lambda = 0.025$ compressive step strain every 500 s, superposed by a small-amplitude oscillatory shear (SAOS) with an imposed shear strain of $\gamma_0 = 0.005$. Large-amplitude oscillatory shear (LAOS) experiments were performed by collecting the steady-state (averaged) waveforms of the stress-strain response at each γ_0 . The elastic stress $\sigma'(t)$ and viscous stress $\sigma''(t)$ contributions to the total stress $\sigma(t)$ were isolated from the total stress response using MITlaos.

The mixtures to form composite hydrogels were loaded onto the MCR-302 (25 mm parallel plate) or the DHR-3 (20 mm parallel plate), and allowed to undergo gelation for 3 hours before compression and shear characterization (gelation profile in Fig. S21). Regular stainless steel plates

were used for characterizing composite hydrogels as we observed minimal differences when using sandpaper (Fig. S11). Tissue samples were loaded onto the MCR-302 (10 mm parallel plate) or the DHR-3 (8 mm parallel plate) which were coated with ultrafine sandpaper (Trizact A10, 3M) to minimize slip effects. Tissue samples were loaded until a normal force of 0.1 N was reached, and trimmed around the rim of the plate before proceeding with analysis. Both the composite hydrogel and tissue samples were sealed in mineral oil to prevent dehydration during testing.

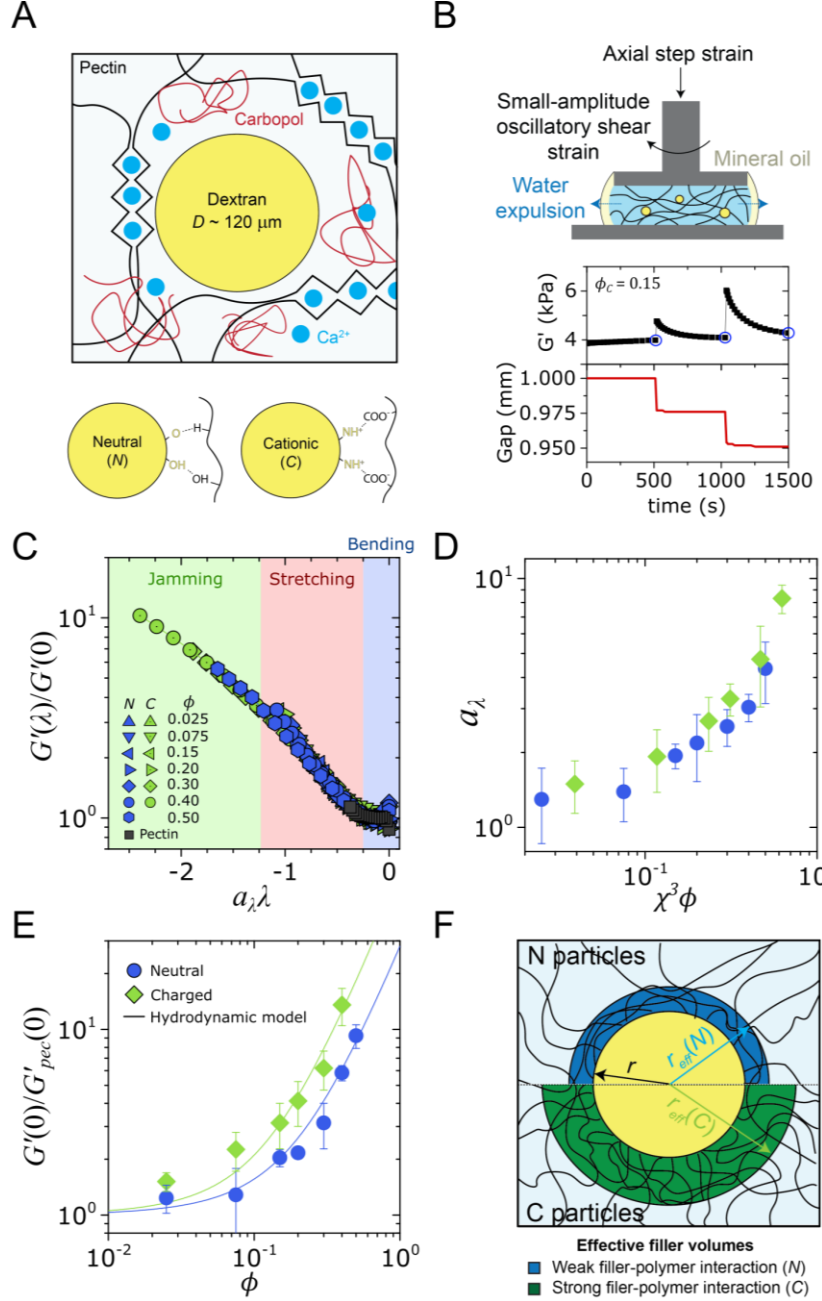


Figure 1. Compression stiffening universality in composite hydrogels. A) Illustration of the composite hydrogel microstructure. The system consists of low-methoxy pectin cross-linked by Ca^{2+} ions, Carbopol, and either neutral or cationically charged dextran particles that undergo weak (H-bonding) and strong (ionic) interactions with the anionic pectin chains. The diameter D of the particles is measured through microscopy imaging (Fig. S1). B) Illustration of the experimental protocol, adapted from reference³. Time-dependent small-amplitude oscillatory shear (SAOS) is superposed on a step axial strain λ . The resulting storage modulus G' is monitored for 500 s (to allow poroelastic equilibration⁵⁹), and the last data points at each step (blue circle) are reported. The hydrogels are almost completely compressible under these conditions, as shown in Fig. S3. C) Representative master curve of normalized G' (relative to the modulus at zero compressive strain, $G'(0)$) as a function of λ shifted by the compressive strain amplification factor a_λ , for the composite hydrogel system as a function of ϕ and ε (see Fig. S6

for repeat set of data). The corresponding regimes of bending (softening in G' with λ), stretching (sharp increase in G' with λ), and jamming (decrease in slope of G' with λ) illustrated by Mackintosh et al.,⁹ are highlighted. D) Compressive strain amplification factor a_λ as a function of $\chi^3 \phi$, where $\chi(C) = r_{\text{eff}}(C)/r_{\text{eff}}(N) = 1.16$, and $\chi(N) = 1$. Statistics ($n = 4$) is obtained from a_λ collected across two sets of experiments (Fig. 1C and S6). E) Linear elasticity of the composite hydrogels at no axial strain $G'(0)$, normalized to that of the pectin hydrogel $G'_{\text{pec}}(0)$, and fitted to the Guth-Gold ($c_2 = 14.1$) hydrodynamic model in Eqn. 1, from which r_{eff} (and thus χ) is obtained. Statistics ($n = 4$) is obtained from compression as well as shear experiments. F) Schematic illustration of the attraction-dependent polymer densification around the filler particles, which results in different effective filler volumes for the neutral and cationic dextran particles in the pectin hydrogels.

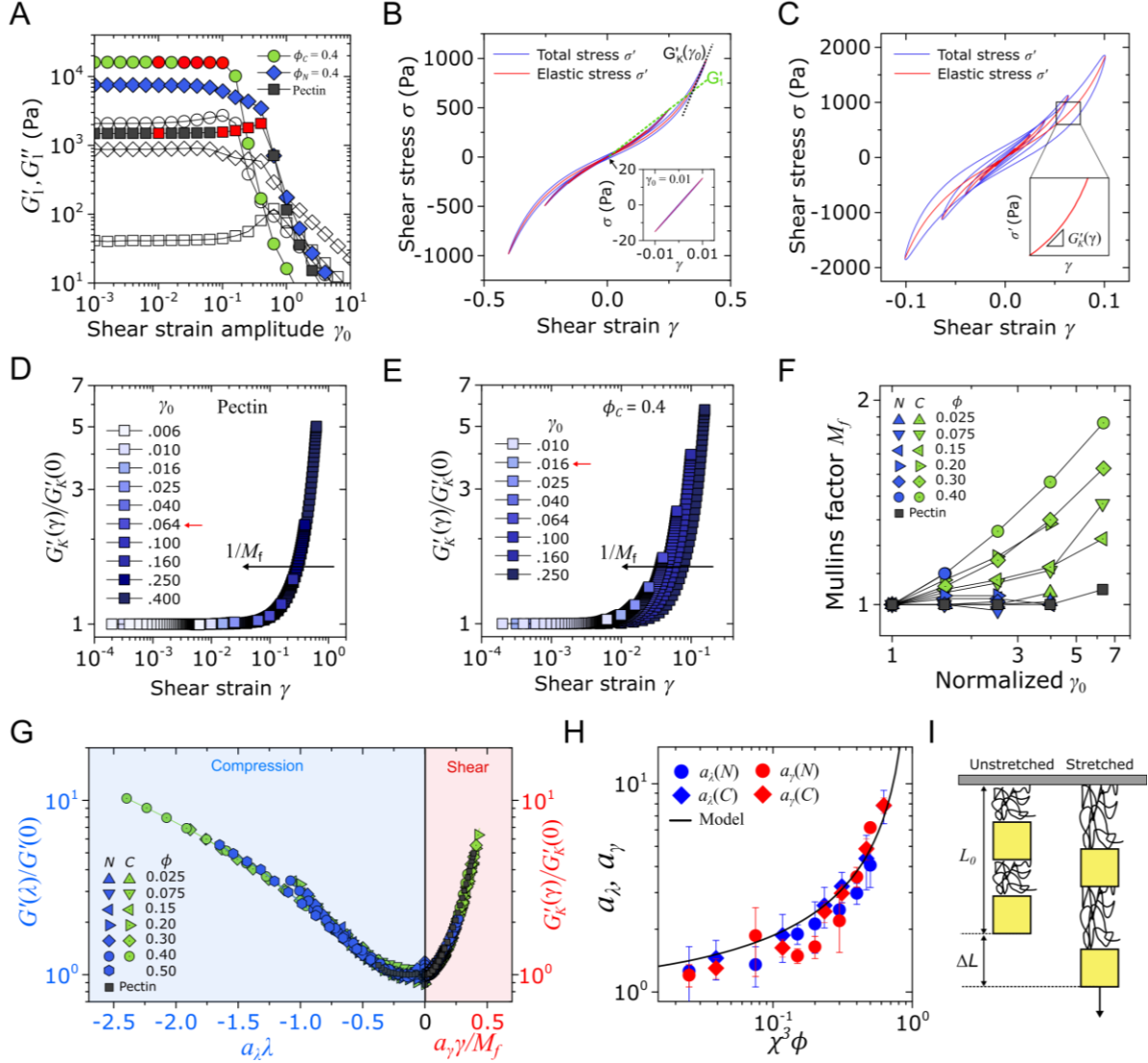


Figure 2. Shear stiffening universality in composite hydrogels. A) The first-harmonic storage modulus G'_1 and loss modulus G''_1 as a function of oscillatory shear strain amplitude γ_0 for pectin and representative composite hydrogels. B), C) Representative Lissajous curves of pectin and $\phi_c = 0.4$ hydrogels at γ_0 corresponding to those highlighted in red symbols in panel A. The Lissajous curves are ellipsoidal at low γ (panel B inset), but become distorted in the non-linear regime. The first-harmonic storage modulus G'_1 is computed from a linear fit from the origin (green dashed line), while the differential storage modulus $G'_K(\gamma_0)$ is computed from the tangent slope at γ_0 (black dotted line), both illustrated in panel B. Our protocol for calculating the *strain-dependent differential storage modulus* $G'_K(\gamma)$ is highlighted in panel C. D), E) The $G'_K(\gamma)$ of the pectin and $\phi_c = 0.4$ gels, normalized by $G'_K(\gamma = 0)$. All data are subsequently shifted to a reference curve measured at γ_0 at which the $G'_K(\gamma)/G'_K(0)$ exhibits a 5% increase (red arrow), and show an exact overlay (see Fig. S13). F) The Mullins factor M_f for the pectin and composite hydrogels as a function of γ_0 (normalized to the reference γ_0) for each system. G) Universal master curve for the composite hydrogels in compression and in shear, and H) corresponding strain amplification factors a_λ and a_γ as a function of $\chi^3\phi$, where $\chi(C) = r_{eff}(C)/r_{eff}(N) = 1.16$, and $\chi(N) = 1$. Statistics for the shear experiments ($n = 4$) are obtained from two sets of experiments, (master curve and Mullins factors of repeat experiments in Fig. S14). I) Illustration of the 1-D affine strain amplification model²⁹ highlighted in panel H. Total strain is defined as $\lambda_{tot} = \Delta L/L_0$, but the polymeric components of the system experience a strain of $\lambda_{pol} = \Delta L/L_0(1 - \phi^{1/3})$. Thus, strain is amplified by a factor $a = \lambda_{pol}/\lambda_{tot} = 1/(1 - \phi^{1/3})$ (Eqn. 2).

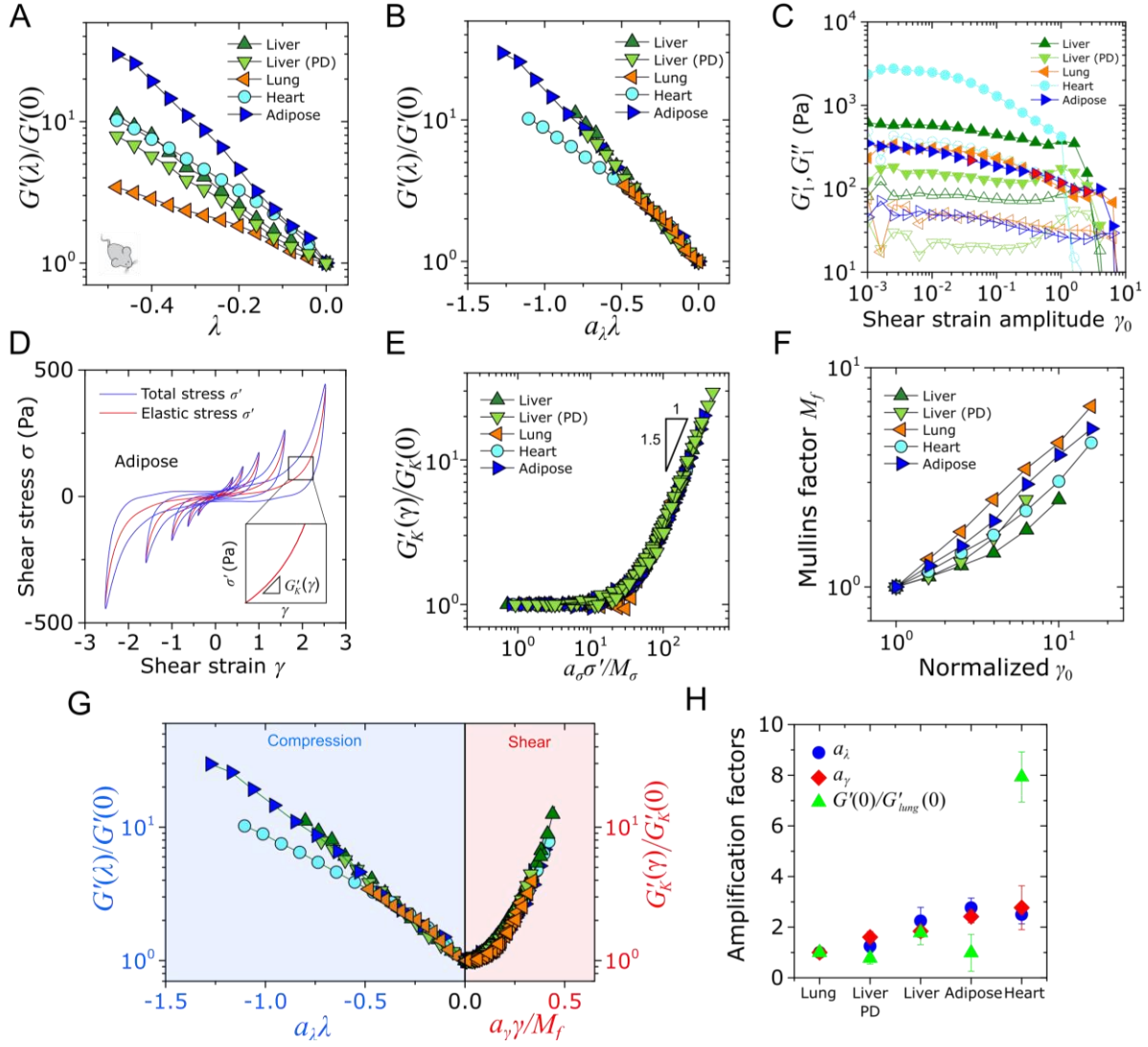


Figure 3. Compression and shear stiffening universality in soft biological tissues. A) Compression stiffening of soft tissue samples from mice (representative pictures in Fig. S16), which is B) shifted to the least stiffening lung sample using the compressive strain amplification factor a_λ . The heart data shows an inflection in the curve with λ , which can be attributed to the round shape of the sample (Fig. S16A) that causes bulging resistance at initial stages of compression (Fig. S17D). C) The first-harmonic storage modulus G'_1 and loss modulus G''_1 as a function of oscillatory shear strain amplitude γ_0 for tissue samples. D) Representative Lissajous curves of adipose tissue at γ_0 corresponding to the red symbols in panel C. Inset illustrates the calculation protocol for the strain-dependent differential storage modulus $G'_K(\gamma)$. E) The master curve of $G'_K(\gamma)$ for different tissues as a function of the elastic stress σ' (see Fig. S19 for discussion of the related shift factors a_σ and M_σ). F) Obtained Mullins factor M_f for the different tissue samples (see Fig. S21B for repeat data). G) Universal master curve for the tissue samples in compression and in shear, and H) the corresponding strain amplification factors a_λ and a_γ , plotted alongside $G'(0)/G'_{lung}(0)$. All curves are shifted to the lung reference curve. Statistics for panel H ($n = 4$) are obtained from repeat experiments (Fig. S21).

SUPPLEMENTARY INFORMATION

Table of Contents

Determination of added dextran mass to the composite hydrogels.....	14
Stabilizing dextran particles from sedimentation in the composite hydrogels.....	15
Dispersion of dextran particles in the composite hydrogels	16
Compressibility of the composite hydrogels.....	17
Stiffening of composite hydrogels under quasi-static compression.....	18
Compression stiffening master curves from repeat experiments	19
Determination of the jamming threshold	19
Fitting the linear elasticity of composite hydrogels with the Batchelor-Green hydrodynamic model.....	20
Differential modulus characterization of pectin and composite hydrogels.....	21
Filler-polymer interaction-dependent Mullins effect in the composite hydrogels	22
Effects of sandpaper on compression and shear rheological characterization	24
Characterization of the occurrence of slip during LAOS experiments	24
Collapse of shear stiffening curves for pectin and composite hydrogels.....	26
Shear stiffening master curves from repeat experiments	26
Comparison between strain amplification and elasticity	27
Representative pictures of tissue samples studied	28
Compressibility of tissues	29
Elastic stress dependence of the differential modulus of pectin and composite hydrogels.....	30
Shifting protocol to obtain elastic stress dependent master curves.....	31
Shear strain stiffening of tissues	32
Results from repeat experiments on tissues	33
Representative gelation plot of pectin and composite hydrogels.....	34

Determination of added dextran mass to the composite hydrogels

The requisite masses of dextran particles to be added were determined based on the required volume fraction ϕ of the swollen particles. The swelling ratio of dextran was determined using two independent methods.

The first method involved calculating the mass difference between dry and swollen particles. To weigh the swollen particles, dextran was allowed to swell in H₂O overnight, after which the solution was centrifuged (5000 g, 10 mins) and poured on a wet filter paper (Whatman Grade 1) on which the mass balance has been zeroed. Excess water was allowed to percolate, and then the final mass of the swollen dextran was determined ($n = 3$). The mean density value of dextran reported in literature ($\rho = 1.09 \text{ g cm}^{-3}$),⁶⁰ to determine the final volumetric swelling ratio of dextran (443 %).

The second method involved calculating the volume ratio between dry and swollen particles by microscopy imaging. The swollen particles were imaged after swelling dry particles in H₂O for 3 hours (same duration as gelation time). Calculation of the swelling ratio based on the differences in the particle sizes yielded an average swelling ratio of 422 %, in reasonable agreement with the mass method. Composite hydrogels with $\phi = 0.15$ were also imaged to determine the particle swelling ratio in the pectin gel; this control experiment reveals that the swelling ratio of the particles is negligibly affected by the particles being inside a hydrogel (Fig. S1).

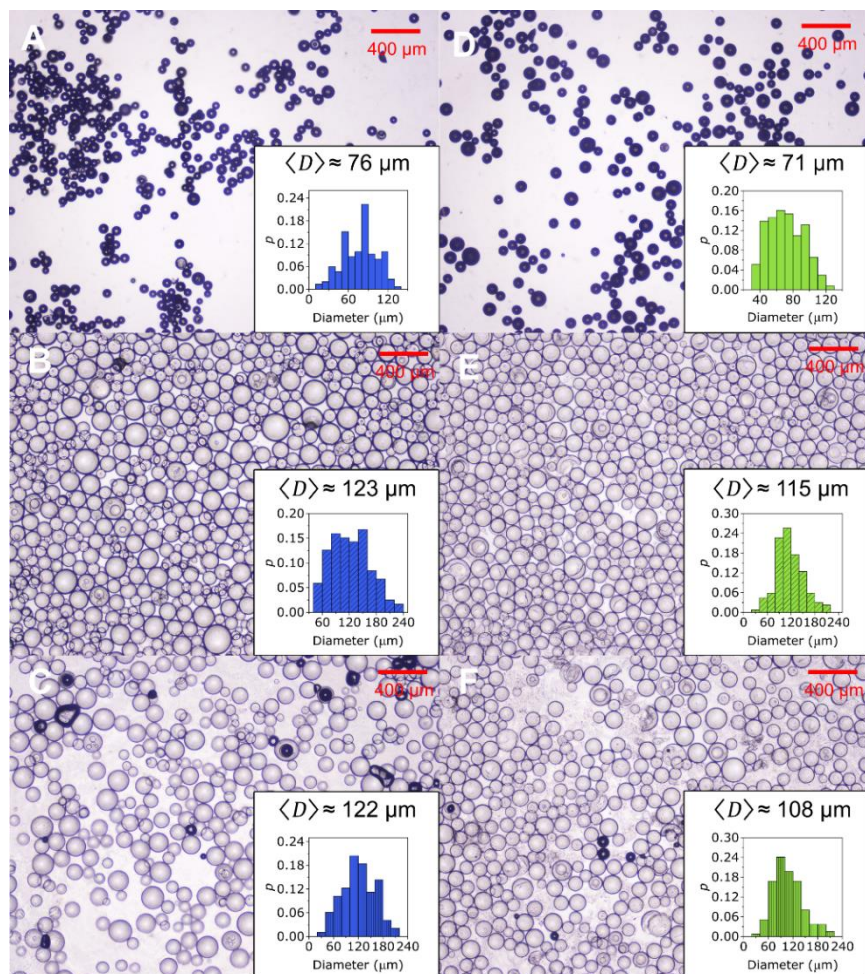


Figure S1. Representative microscope images (Olympus CKX53) of neutral dextran particles in the A) dry and B) swollen state, and C) in a $\phi = 0.15$ gel state, and cationic dextran particles in the D) dry and E) swollen state, and F) in a $\phi = 0.15$ gel state. Note that the ϕ values refer to the concentration of dextran added to make the gel, and not the ϕ in the image (as the gels were imaged by compressing the hydrogels between microscope slides). Representative particle size distributions ($n = 100$) as well as the associated mean diameter $\langle D \rangle$ are shown in the inset.

Stabilizing dextran particles from sedimentation in the composite hydrogels

We found that the addition of a yield stress fluid to be essential in creating hydrogels with stabilized particles. In the absence of yield stress fluids, we found that the particles exhibited sedimentation during gelation (Fig. S2A). Particle sedimentation can significantly affect compression stiffening in the composite hydrogels, as compressive strain will mainly result in a particle jamming response. To prevent the sedimentation of the dextran particles, we incorporated Carbopol 940 (0.5 wt. % total concentration) in the hydrogel, which results in the stabilization of the particles during gelation (Fig. S2B).

The Carbopol solution prevents dextran particle sedimentation by resisting the gravitational force of the particles. The yield stress of Carbopol at 0.5 wt. % can be analyzed through a flow curve analysis (Fig. S2C). A fit to the Herschel-Bulkley model:

$$\sigma = \sigma_y + K\dot{\gamma}^n \quad (0.1)$$

where σ_y is the yield stress, K is the consistency index, and n is the flow index, shows that the Carbopol solution has a yield stress of $\sigma_y = 0.93$ Pa. The gravitational force of the dextran particles F can be computed by the relation $F = (4/3)\pi gr^3(\rho_{dex} - \rho_{H_2O})$, where $g = 9.8 \text{ ms}^{-2}$ is gravitational acceleration, $r \approx 60 \text{ }\mu\text{m}$ is the radius of the dextran particles (see Fig. S1), and $\rho_{dex} = 1090 \text{ kgm}^{-3}$ is the density of dextran, and ρ_{H_2O} is the density of water. F can now be compared to the yield stress of the surrounding fluid, σ_y , via the relation:

$$Y_g = \frac{2\sigma_y\pi r^2}{F} \quad (0.2)$$

where Y_g is the gravitational yield number. The Y_g of dextran particles in the Carbopol solution $Y_g = 26.3$, which is substantially higher than the Beris criterion⁶¹, which states that spherical particle sedimentation occurs when $Y_g < 0.143$. This calculation assumes that the particles do not directly aggregate, which we discuss in the next section.

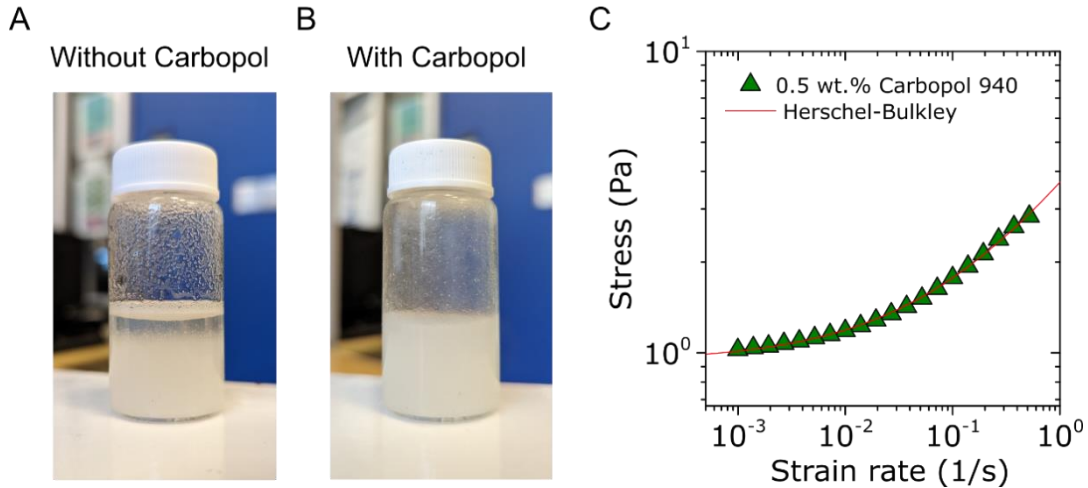


Figure S2. Yield stress fluids in the matrix prevent dextran particle sedimentation. Representative pictures of the composite hydrogels A) without Carbopol and B) with Carbopol (0.5 wt. %), in 20 mL scintillation vials. C) Flow curve of a 0.5 wt. % solution of Carbopol, fitted to the Herschel-Bulkley model.

Dispersion of dextran particles in the composite hydrogels

We find that dextran does not directly undergo particle-particle aggregation in our composite hydrogels. The large size of the dextran particles ($D \approx 120 \mu\text{m}$) and lack of specific interactions between two particles should result in a preferential interaction with the polymer matrix which offers multivalent binding sites for the particles – this is especially so for the cationic dextran particles. To demonstrate that the particles do not exhibit aggregation, we imaged $\phi_N = 0.01$ and $\phi_C = 0.01$ composite hydrogels which were gelled in a square capillary (Vitrocom) and sealed with a mixture of Vaseline-lanolin-paraffin. The images show that the particles are generally well-dispersed with minimal direct contact (Fig. S3). The particles do exhibit proximity however, which can be attributed to bridging interactions in the system. The images also show that particles exhibit minimal interpenetration with each other – a behavior which can result in non-linear elastic behavior from the particles even without the polymer matrix⁶².

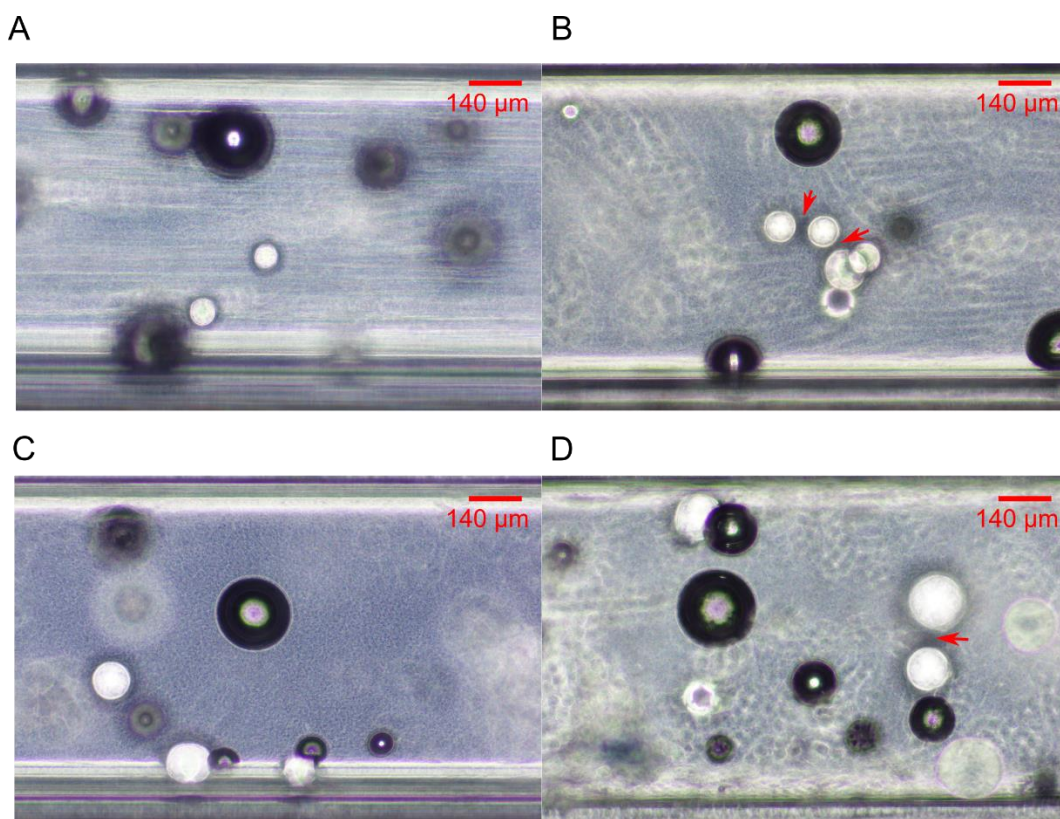


Figure S3. Representative microscope images (Olympus CKX53) of A,B) $\phi_N = 0.01$ and C,D) $\phi_C = 0.01$ composite hydrogels, all gelled in 0.9 mm width x 0.9 mm thickness square capillaries (Vitrocom). Note that the particles are in various states of focus due to the thickness of the capillary sample. Some of the particles in the same line of focus exhibit proximity without direct contact (red arrows), which may be attributed to polymer-induced bridging interactions.

Compressibility of the composite hydrogels

We calculated the Poisson's ratio ν of our gel systems by tracking the transverse strain that arises during the quasi-static axial compression experiments. This was done through a camera setup placed under a clear rheometer plate, with gels dyed red using food coloring (Fig. S4A). The perimeters of the gels were then identified using MATLAB, and fitted to a circle to obtain the radius as a function of axial strain, and thus transverse strain. The Poisson's ratio ν was calculated via the relation $\nu = \lambda_{trans}/\lambda_{axial}$.

The composite hydrogels are almost completely compressible, with $\nu \sim 0$. The pectin hydrogels with Carbopol display a moderate amount of radial expansion ($\nu = 0.2$), but we find that this can be mostly attributed to the Carbopol, as pectin hydrogels without Carbopol also exhibits $\nu \sim 0$. The complete compressibility of the gels shown here is similar to that observed in biopolymer networks,^{37,59,63} which would indicate that both the pectin and composite hydrogels exhibit fairly large pore sizes (despite the short persistence length of pectin, and despite the kPa scale elasticity of these systems).

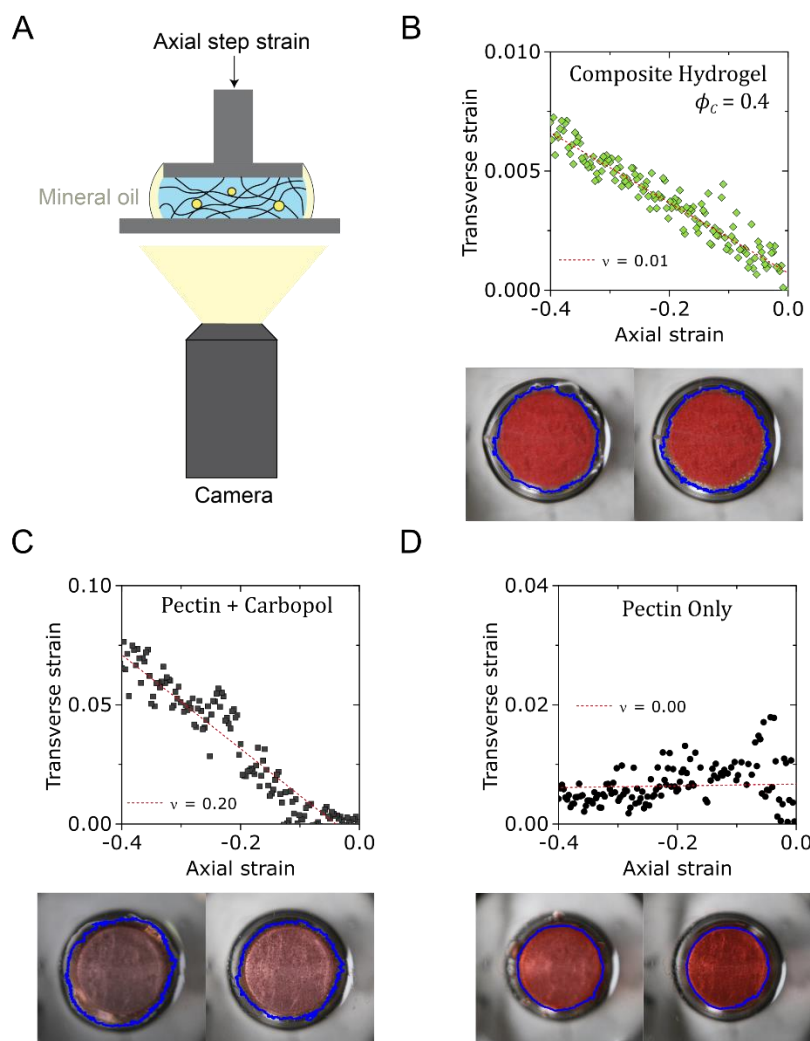


Figure S4. Analysis of gel compressibility under quasi-static axial strains. A) Schematic illustration of the setup used to analyze the radial expansion of the gel systems under compression. All experiments were done using a 20 mm parallel plate geometry (DHR-3). Transverse and axial strains of B) composite hydrogels with $\phi_c = 0.4$, C) pectin hydrogels with Carbopol, and D) pectin hydrogels without Carbopol. The slope was used to calculate the Poisson's ratio ν . The images under each graph show the pictures of the gels – dyed red with food coloring – before (right) and after (left) the compression experiments. The blue outline illustrates the perimeter of the gel as identified using MATLAB, with which transverse strain is calculated.

Stiffening of composite hydrogels under quasi-static compression

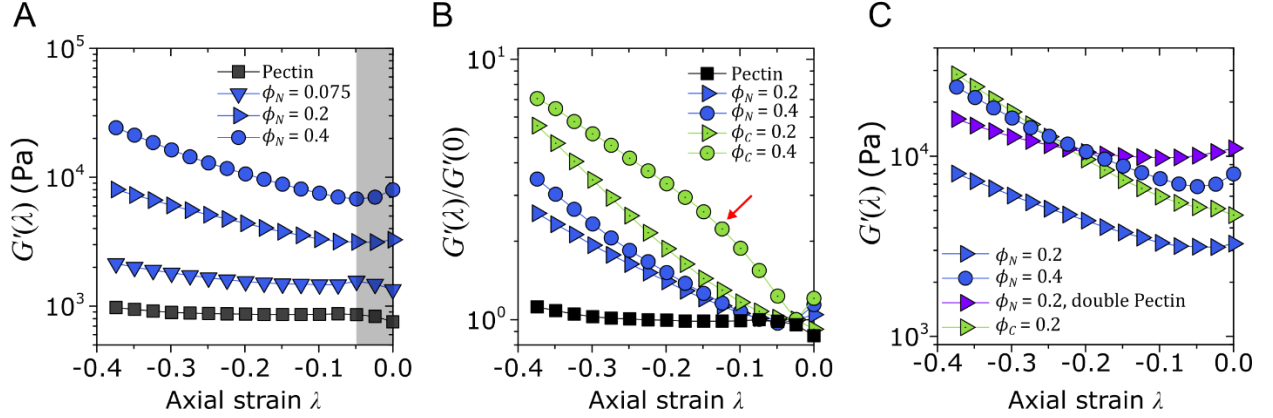


Figure S5. Representative storage modulus G' as a function of compressive axial strain λ for the composite hydrogel (all systems contain Carbopol). A) $G'(\lambda)$ of the pectin hydrogel, and of the composite hydrogel with N particles at various volume fractions. Both the linear shear modulus, $G'(\lambda = 0)$, and the extent of compression stiffening are observed to increase with ϕ . The anomalous behavior observed at low λ are shaded in the panel. The initial stiffening behavior in the pectin and $\phi_N = 0.075$ may arise due to the relatively high Poisson ratio ν of the gels at ϕ_N (Fig. S4C), since this can cause buckling (which in turn can cause stiffening⁶⁴) prior to sample expulsion. The initial softening behavior at $\phi_N = 0.2$ and $\phi_N = 0.4$ are expected behaviors arising from chain buckling in compressed biopolymer networks⁶³. We normalize our data after the initial softening regime subsequent figures (panel B, Fig. 1C) to focus on the emergent stiffening behaviors in the composite hydrogels. B) The storage modulus values normalized by $G'(0)$ (the G' value after the initial anomalous regime) for composite hydrogels with varying interaction strength ε . The hydrogels with charged particles exhibit more substantial compression stiffening across all ϕ . At high ϕ , there is a knee point in the slope of the curve (red arrow), which characterizes the onset of the jamming regime. C) Comparison of $G'(\lambda)$ values for composite hydrogels with varying ε as well as polymer concentration. The $\phi_C = 0.2$ gel shows a greater compression stiffening effect compared to ϕ_N gels with higher $G'(\lambda = 0)$ (the $\phi_N = 0.4$ as well as $\phi_N = 0.2$ with 2 wt. % of pectin), showing that compression stiffening does not directly correlate with the elastic modulus of the gels.

Compression stiffening master curves from repeat experiments

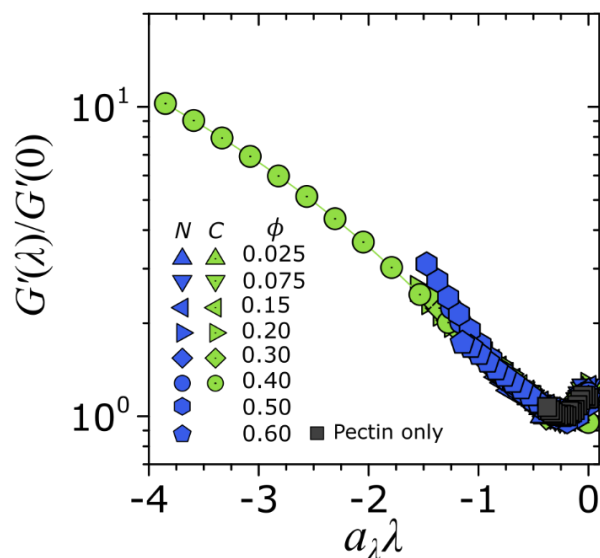


Figure S6. Second compression stiffening master curve from repeat experiments.

Determination of the jamming threshold

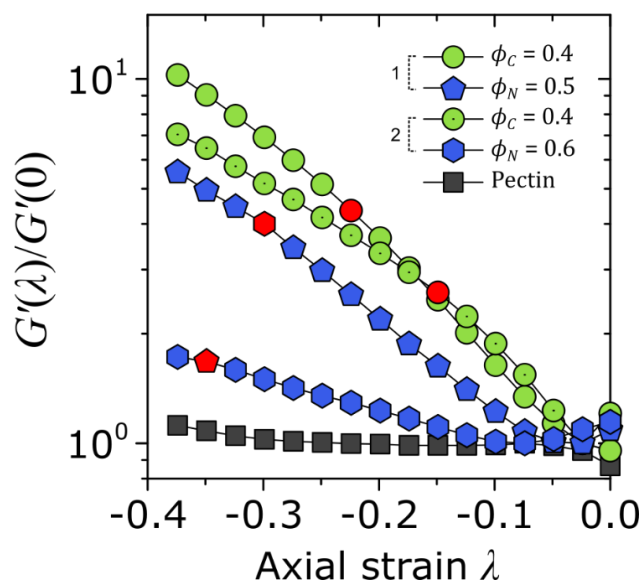


Figure S7. Normalized G' of composite hydrogels at volume fractions ϕ exhibiting jamming behavior (across two sets of experiments per ϕ). The jamming threshold strain λ_{jam} is identified by calculating the knee point of each curve, and is highlighted in red for each curve.

Fitting the linear elasticity of composite hydrogels with the Batchelor-Green hydrodynamic model

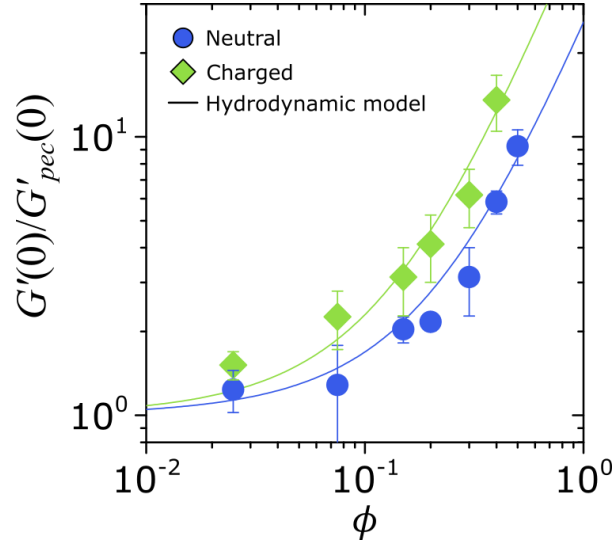


Figure S8. Same data as Fig. 1E, fitted instead to the Batchelor-Green ($c_2 = 5.2$) variant¹⁴ of the hydrodynamic model in Eqn. 1. The resulting $\chi = (\phi_{jam}(N)/\phi_{jam}(C))^{1/3} = 1.17$.

Differential modulus characterization of pectin and composite hydrogels

We characterized the non-linear elasticity of the pectin and composite hydrogels by first characterizing the differential storage modulus, in which the terminal slope of the elastic stress σ' was measured for each Lissajous cycle (Fig. 2B,C), thus providing $G'_K(\gamma_0) = (d\sigma' / d\gamma)|_{\gamma_0}$. The analysis of this quantity for the pectin and composite hydrogels shows that the composite system exhibits a softer response than the matrix pectin hydrogel (Fig. S9A,B). We also followed the more conventional route to obtaining the differential storage modulus, where a small-amplitude oscillatory shear is superposed onto a step stress σ_0 .^{21,22,65} This form of the differential storage modulus, $K'(\sigma_0)$, was characterized by superimposing a $\sigma = 10 \text{ Pa}$ oscillatory shear at $\omega = 10 \text{ rad/s}$ onto the step stress σ_0 , where the step stress was alternated from an increasing step stress to a zero step stress at 20 s intervals. In general, we found this method to be the least suitable for characterizing the non-linear elasticity of our systems, as failure (or slip) occurs much earlier than from LAOS-based methods (Fig. S9C). We hypothesize that this may be due to the greater overall work put into the system by the step stress protocol compared to LAOS, and due to the fact that our materials are much stiffer than the biopolymer networks which are typically studied using this method.

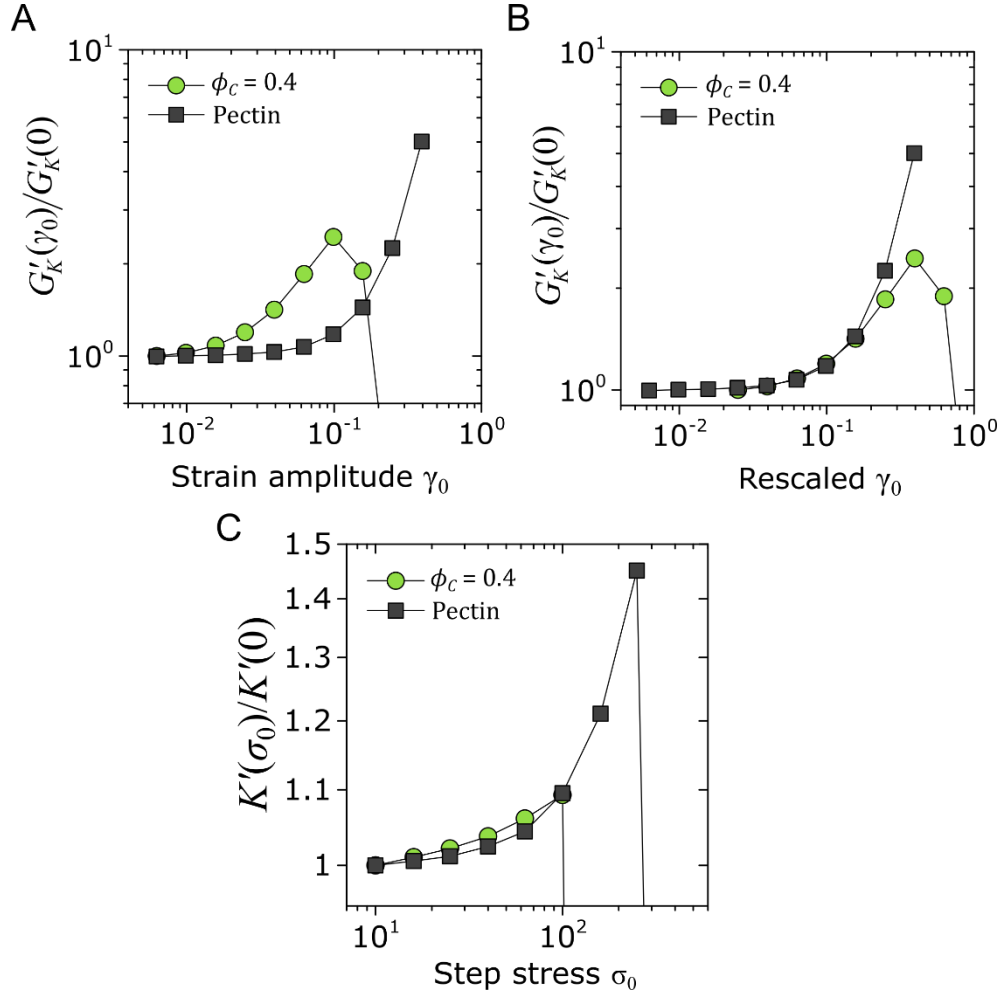


Figure S9. A) Normalized differential storage modulus $G'_K(\gamma_0)$ of the pectin and $\phi_c = 0.4$ composite hydrogels. B) Same data, but the $\phi_c = 0.4$ data is horizontally shifted onto the pectin data. C) Normalized differential storage modulus $K'(\sigma_0)$ obtained using the step stress protocol.

Filler-polymer interaction-dependent Mullins effect in the composite hydrogels

We performed explicit characterization of the Mullins effect, which refers to the stress softening that is observed in composite systems in response to increasing cyclic strain (Fig. S10A). A distinguishing feature of systems exhibiting the Mullins effect is that the loading curves of the subsequent cycle traces the unloading curve of the previous cycle, resulting in measurable quantities such as dissipation (purple arrows, Fig. S10B,C) and plastic deformation (purple arrows, Fig. S10D,E).^{4,52,66} The high- ϵ composite hydrogels with *C* fillers exhibit significantly greater Mullins effect than those with *N* fillers, indicating that strong filler-polymer interactions result in greater polymer adsorption on the fillers, and thus greater elastoplastic dissipation.²⁹

As the LAOS experiments also involve increasing cycling strain, we should be able to observe some traits of the Mullins effect in LAOS for the *C*-filled hydrogels. We indeed find that the maximum shear strain of the previous cycles approximately corresponds to the knee point of the subsequent elastic stress curves (Fig. S10F) (they are in fact slightly higher, which is consistent with Fig. S10B). We also measured transient Lissajous curves (i.e., as opposed to the steady state curves presented in the paper) and indeed find that loading curves of subsequent cycles trace the unloading curves of the previous cycles (Fig. S10G).

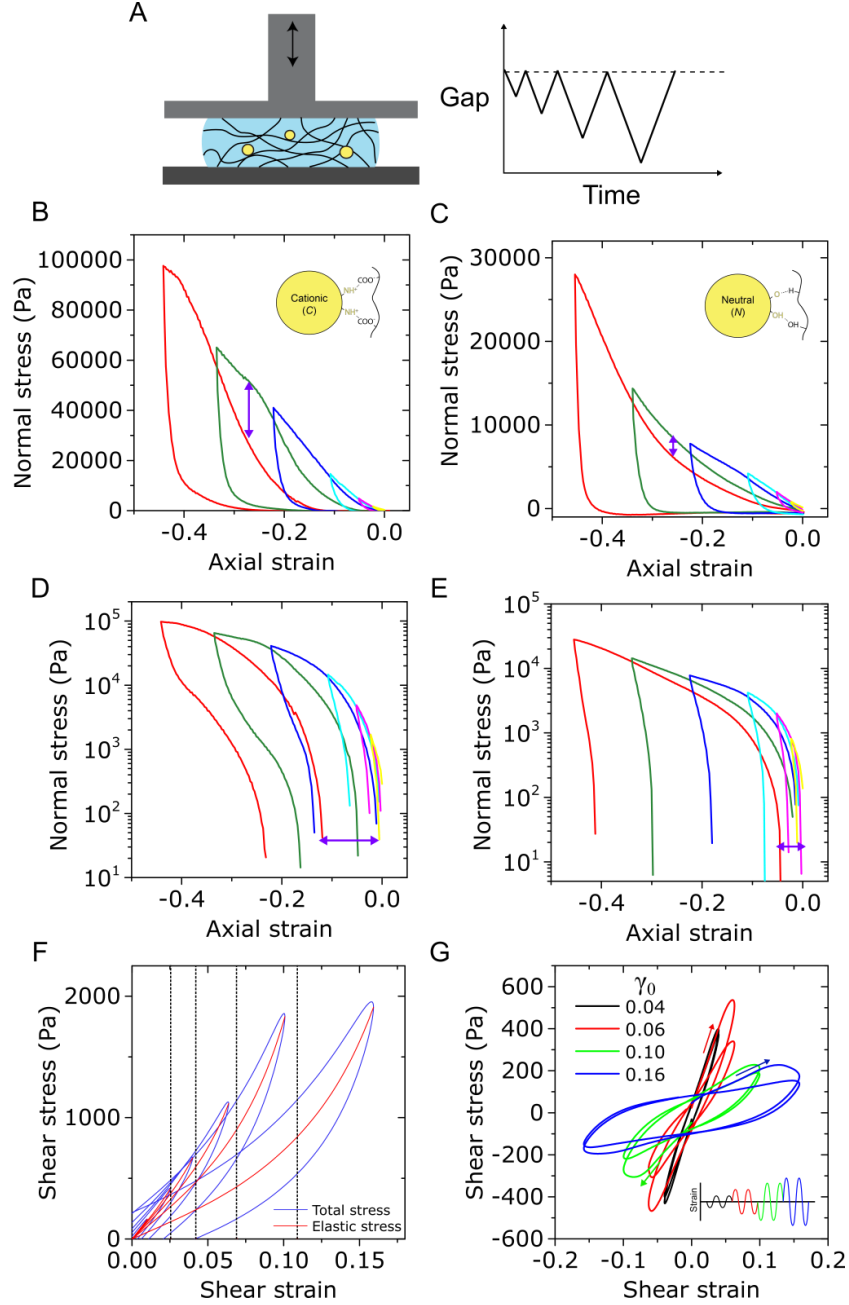


Figure S10. Mullins effect characterization of the composite hydrogels. A) Method of analysis. Composite hydrogels with N and C fillers were gelled in disc molds (25 mm diameter, 3.6 mm thick), after which cyclic compression experiments were conducted on a DHR-3 rheometer (40 mm parallel plate) at a speed of 0.01 mm/s. B,C) Compression stress-strain curves of the C and N filled systems, and D,E) the same plots in semilog axes. The Mullins effect results in dissipation (vertical purple arrows in B,C) and permanent strain (horizontal purple arrows in D,E). F) Lissajous curves of the $\phi_C = 0.4$ gel measured at $\gamma_0 = 0.04, 0.064, 0.10$, and 0.16 . The dashed lines show the knee points of the elastic stress curves. G) Transient Lissajous curves of the $\phi_C = 0.4$ gel measured at $\gamma_0 = 0.04, 0.064, 0.10$, and 0.16 . Each curve shows two cycles, after which the strain direction is flipped (the method is illustrated in the bottom right inset). The arrows show the loading direction of the curves, roughly tracing the unloading curves of their previous curves.

Effects of sandpaper on compression and shear rheological characterization

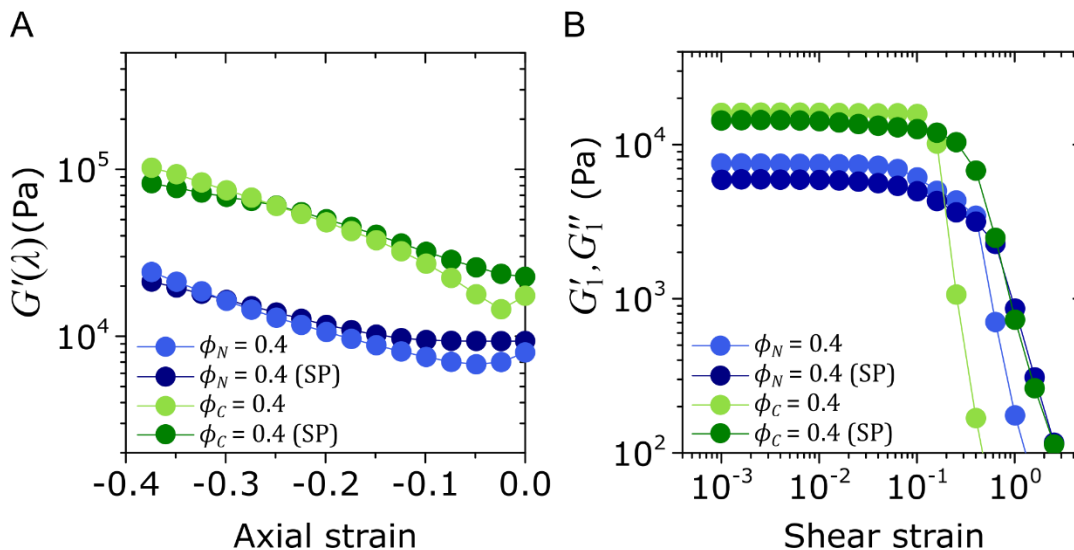


Figure S11. Representative A) compression and B) shear rheological characterization for the composite hydrogels with 60 grit sandpaper (SP) on the rheometer plates. Most experiments in the manuscript are done without sandpaper as we found the difference in the results to be relatively minimal.

Characterization of the occurrence of slip during LAOS experiments

Understanding the role of slip is critical for ensuring that slip effects are not influencing the shear responses of the composite hydrogels, such as the horizontal translation in $\sigma'(t)$ and the shape of the $G'_K(\gamma)$ curves. We find that the N -filled composite hydrogels at high ϕ exhibit clear signatures of slip, as there is a gradual drop in the G' preceding the yielding point (Fig. S12A).²⁶ We also find that the corresponding $G'_K(\gamma)$ curves in the slip regime for $\phi_N = 0.4$ begin to deviate from the G'_K responses of the polymer matrix as well as the $\phi_C = 0.4$ system (Fig. S12B).

We thus find a curious result where the higher ε composite hydrogels are both cohesive (higher elasticity) *and* adhesive (higher slip resistance) – two properties which are conventionally thought to be diametric in adhesion literature. We hypothesize that this can occur because the C fillers are cationically charged, are present on the gel surface, and thus provide greater adhesion to the metal plates of the rheometer (Fig. S12C). To validate this idea, we placed a 10 μ L drop of a mineral oil solution with 2 wt. % of the anionic surfactant AOT, and we indeed find that the droplet completely wetted the C -filled hydrogel, while remaining beaded on the N -filled hydrogel (Fig. S12D). Moreover, to validate that these surface

interactions affect the slip response of the gels, we repeated the LAOS experiments by placing poly(vinyl chloride) (PVC) tape on the rheometer plates, since these plastic surfaces should not facilitate charge-induced adhesion. We find that the N -filled hydrogels exhibit the same LAOS response, and the C -filled hydrogels now exhibit a dramatic slip response characterized by a lowering in the G' (Fig. S12E,F). The analysis of the G'_K response in this slip regime shows that G'_K again deviates from the expected response of the system (Fig. S12G).

Overall, we find that slip results a *lowering* of the $G'_K(\gamma)$ response. This provides a useful context to interpret the tissue experiment results, as while we find that G' and G'' drop as a function of γ_0 (Fig. 3C), the calculated G'_K exhibit a stress scaling of $G'_K(\sigma) \sim \sigma^{1.5}$ which is the expected upper limit of the scaling of G'_K arising from the biopolymer matrix. This suggests that LAOS characterization of tissues are likely not convolved by slip.

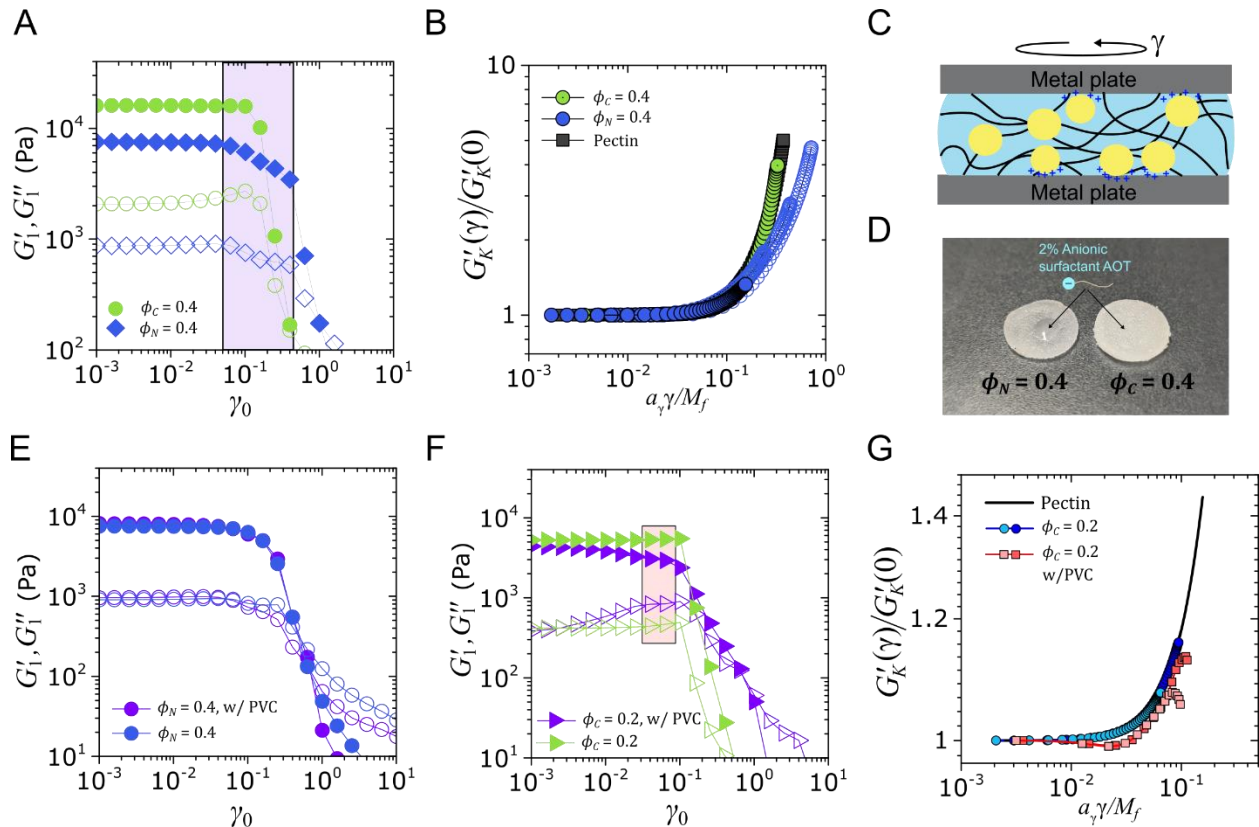


Figure S12. Characterization of slip effects on the composite hydrogels ($\phi = 0.4$). A) First harmonic storage and loss moduli of the composite hydrogels (same data as Fig. 2A), highlighting the region exhibiting slip in the $\phi_N = 0.4$ system. B) Shear stiffening master curve of the pectin and composite hydrogels, where the data for each system is shifted by $1/M_f$ and then all of the data is shifted onto the pectin curve (see Fig. SX for full data). The hollow symbols are $G'_K(\gamma)$ of $\phi_N = 0.4$ gels extracted from the slip region in panel A. C) Schematic illustration of the charge-induced adhesion of the gels onto the rheometer plates facilitated by C fillers. D) Pictures of composite hydrogel discs (25 mm diameter) with a droplet of a solution of mineral oil with 2 wt. % AOT. E,F) First harmonic storage and loss moduli of the composite hydrogels with PVC tape on the rheometer plates. G) $G'_K(\gamma)$ of the C -filled composite hydrogels in the slip region highlighted in panel F using PVC tape, shifted onto the pectin data.

Collapse of shear stiffening curves for pectin and composite hydrogels

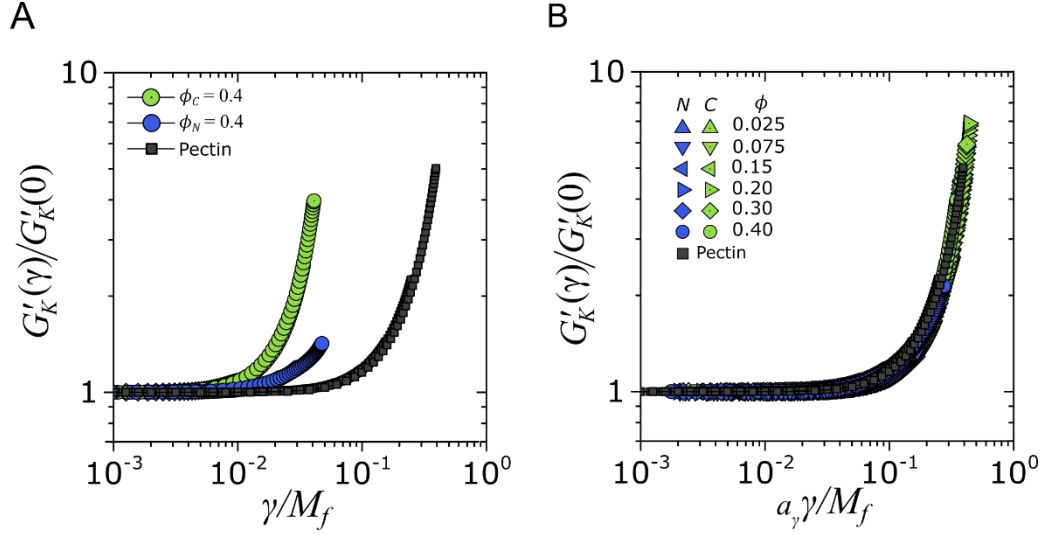


Figure S13. A) Representative examples of the $G'_K(\gamma)$ curves after performing horizontal shifting to account for the Mullins effect (see Fig. 2C,D). The curves are self-similar, but horizontally translated. B) Collapse of $G'_K(\gamma)$ as a function of ϕ and ε using the shear strain amplification factor a_γ .

Shear stiffening master curves from repeat experiments

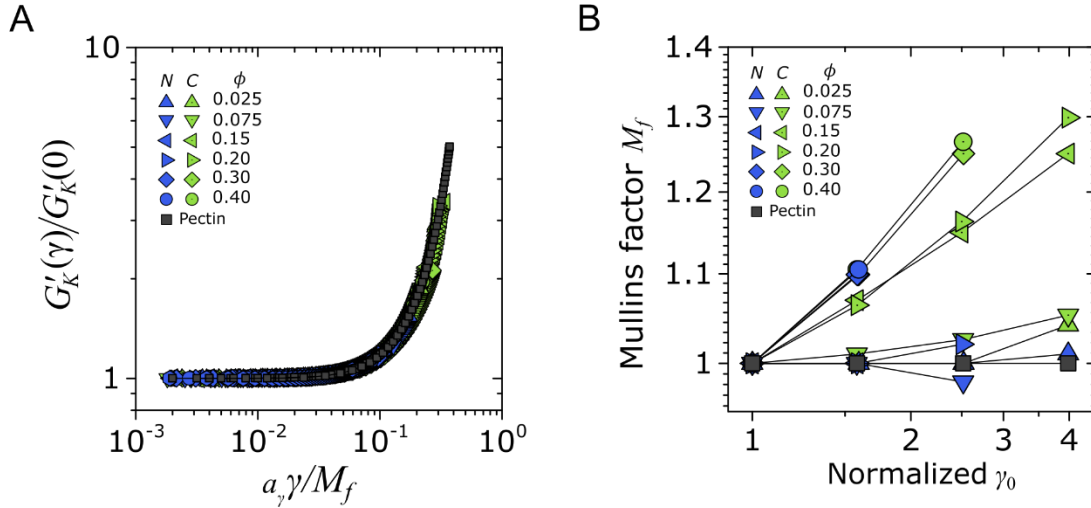


Figure S14. Results from repeated shear experiments. A) Master curve of $G'_K(\gamma)$ as a function of ϕ and ε . The associated shear strain amplification factor a_γ is used to obtain statistics for Fig. 2H in the main manuscript. B) The Mullins factor M_f for the hydrogels as a function of ϕ and ε .

Comparison between strain amplification and elasticity

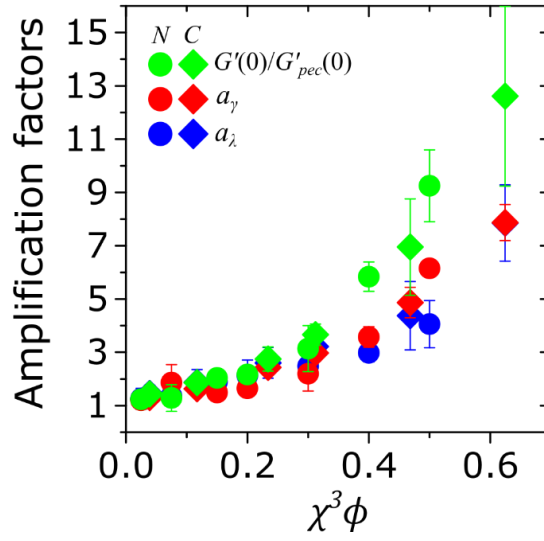


Figure S15. Comparison between the compression and shear strain amplification factors a_λ and a_γ , and the linear elasticity of the system $G'(0)/G'_{pec}(0)$ (shown in linear scale). The strain amplification factors provide a reasonable description of $G'(0)/G'_{pec}(0)$ at $\chi^3\phi < 0.3$, but begin to deviate at higher $\chi^3\phi$.

Representative pictures of tissue samples studied

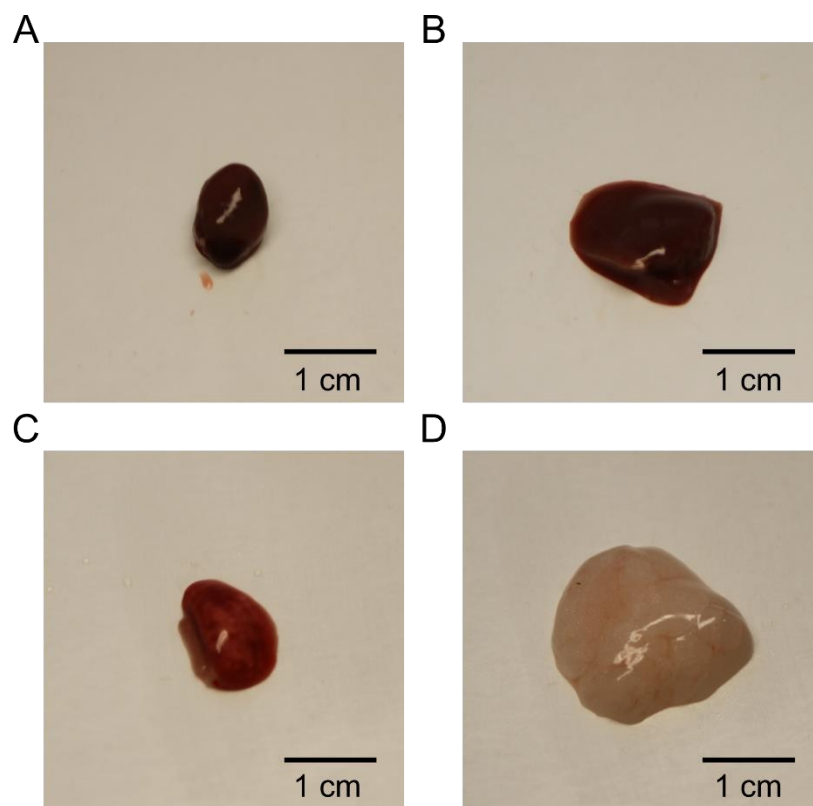


Figure S16. Representative pictures of A) heart, B) liver, C) lung, and D) adipose samples excised from mice.

Compressibility of tissues

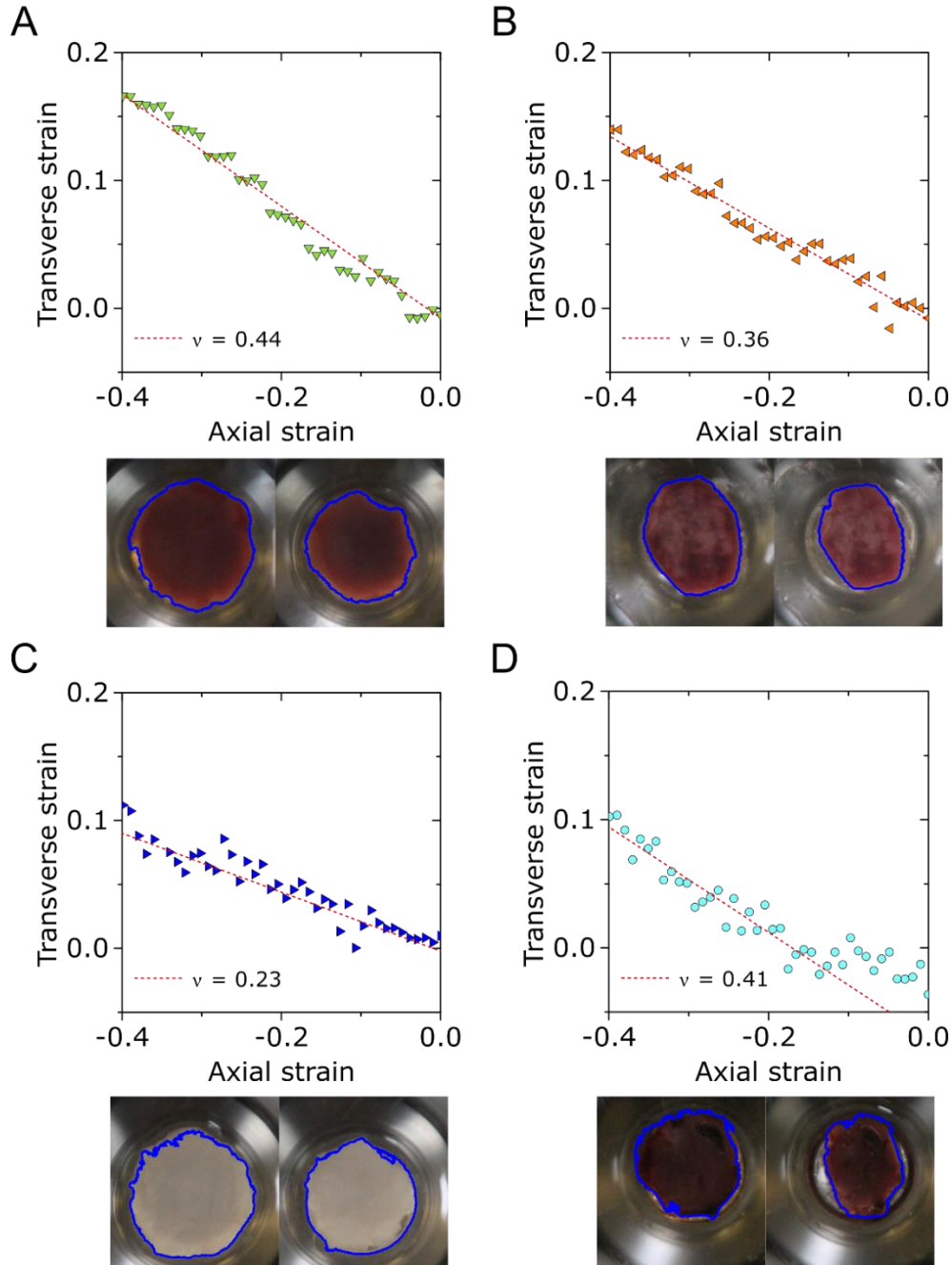


Figure S17. Analysis of tissue compressibility (following protocols illustrated in Fig. S4) for A) liver, B) lung, C) adipose, and D) heart. The Poisson's ratio is calculated by the relation $\nu = \lambda_{trans}/\lambda_{axial}$. The heart sample exhibits a non-linear dependence of transverse strain on axial strain. We find this arising due to the flattening of the heart sample at low strains (the sample is initially round (Fig. S16)); the Poisson's ratio is thus calculated after the initial flattening stage.

Elastic stress dependence of the differential modulus of pectin and composite hydrogels

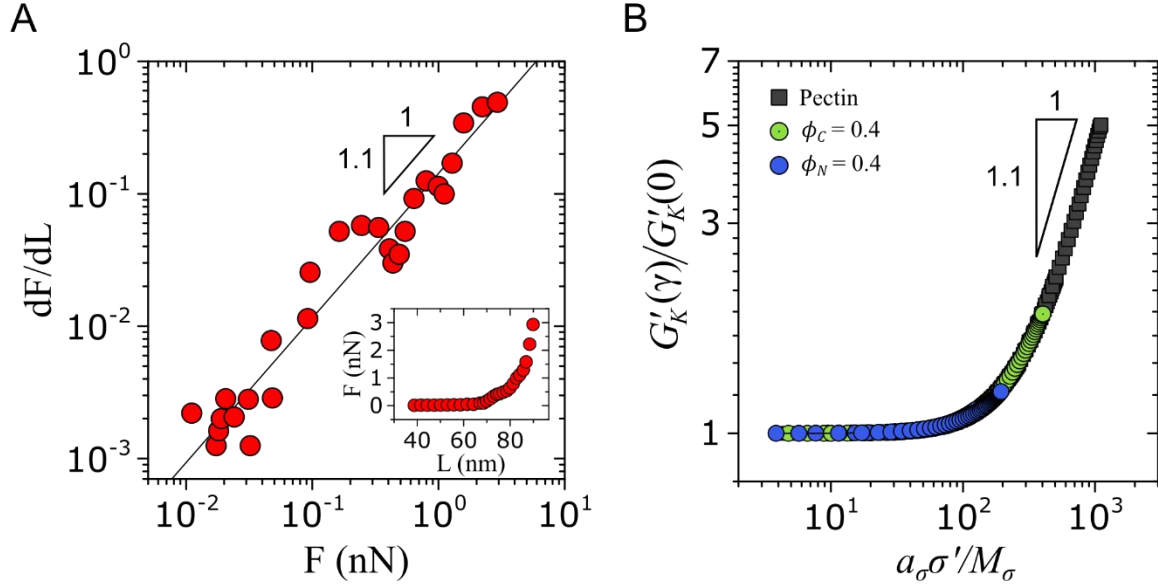


Figure S18. The non-linear elasticity of pectin and composite hydrogels can be attributed to the stretching of the pectin chains. A) Derivative of force F (as a function of displacement L) versus F of pectin hydrogels. Fitting the data to the function $dF/dL \sim F^z$ yields $z = 1.1$. The inset shows the raw F - L data of pectin, retrieved from reference⁴¹. B) The strain-dependent differential modulus of pectin and composite hydrogels plotted as a function of σ' . The terminal slope of the curve follows $G'_K(\gamma) \sim \sigma'^z$. Note that the horizontal axis is rescaled by the stress-induced Mullins effect and the stress amplification factor (see Fig. S19 for discussion about the curve shifting process).

Shifting protocol to obtain elastic stress dependent master curves

The strain-dependent differential storage modulus $G'_K(\gamma)$ can also be explored as a function of elastic stress σ' in similar vein to the classical literature on this topic.^{2,21} The $G'_K(\gamma)$ vs σ' curves exhibit horizontal translation with increasing shear strain amplitude γ_0 – in similar vein to $G'_K(\gamma)$ vs γ curves (Fig. 2D,E) – but the trend is reversed where the curves now show an earlier onset of stiffening with elastic stress (Fig. S19A). This is a manifestation of stress softening, as a lower amount of stress is required to strain the polymer network to its non-linear regime. The associated Mullins shifted factor, M_σ , appears to be inversely related to M_f , but in a non-linear manner (Fig. S19B). The resulting master curves for the different tissues (Fig. S19C) can then be rescaled into a master curve (Fig. 3E), through a stress amplification factor a_σ . This stress amplification factor qualitatively appears to be inversely related to the elasticity of the system (Fig. S19D).

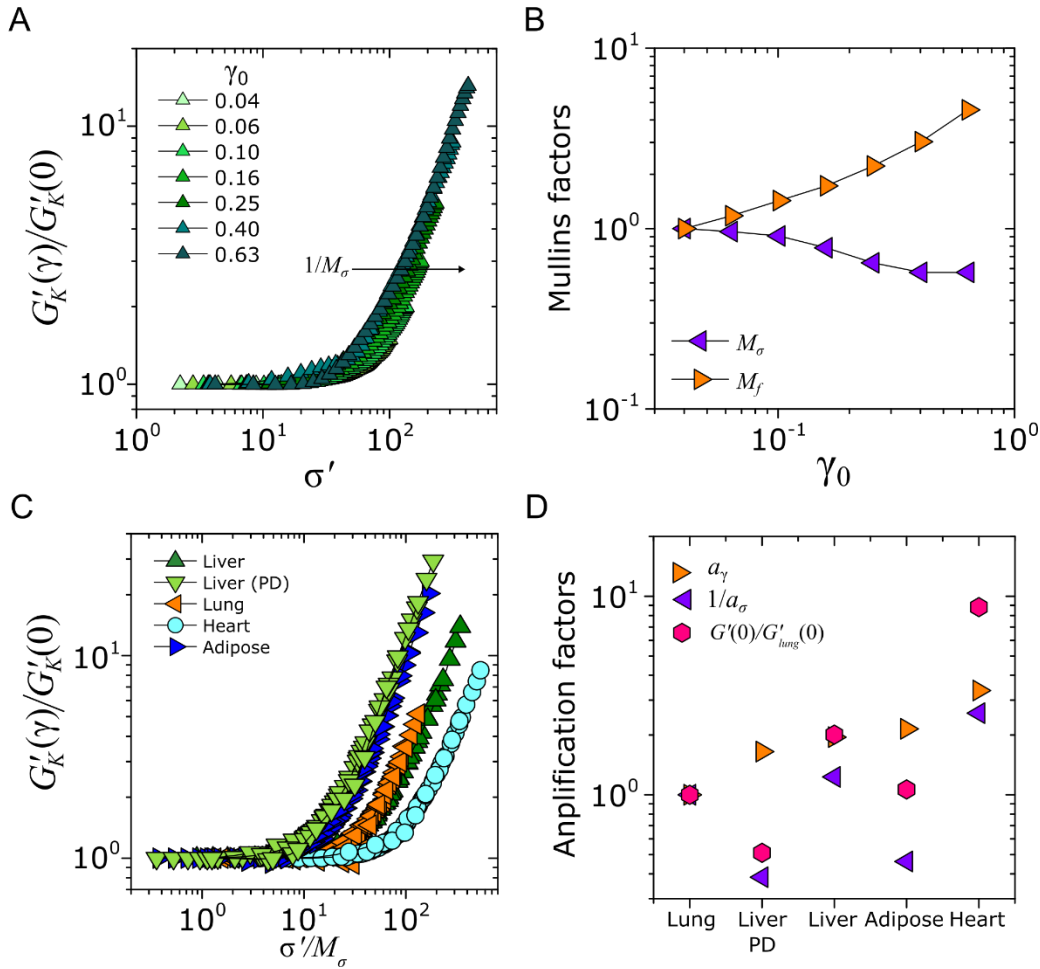


Figure S19. A) Representative $G'_K(\gamma)$ data for heart as a function of σ' . The data is shifted to the reference curve ($\gamma_0 = 0.04$) through the shift factor $1/M_\sigma$. B) Comparison of the strain-based Mullins factor M_f and the stress-based Mullins factor M_σ for the heart sample, showing an approximate inverse (but not linearly inverse) relationship with each other as a function of strain amplitude γ_0 . C) The $G'_K(\gamma)$ vs σ' master curves for the different tissue samples. The shown curves are then horizontally shifted to the lung master curves with the shift factor a_σ . D) Comparison of the strain amplification factor a_γ , stress amplification factor a_σ , and elastic modulus $G'(0)$ normalized by that of the lung system.

Shear strain stiffening of tissues

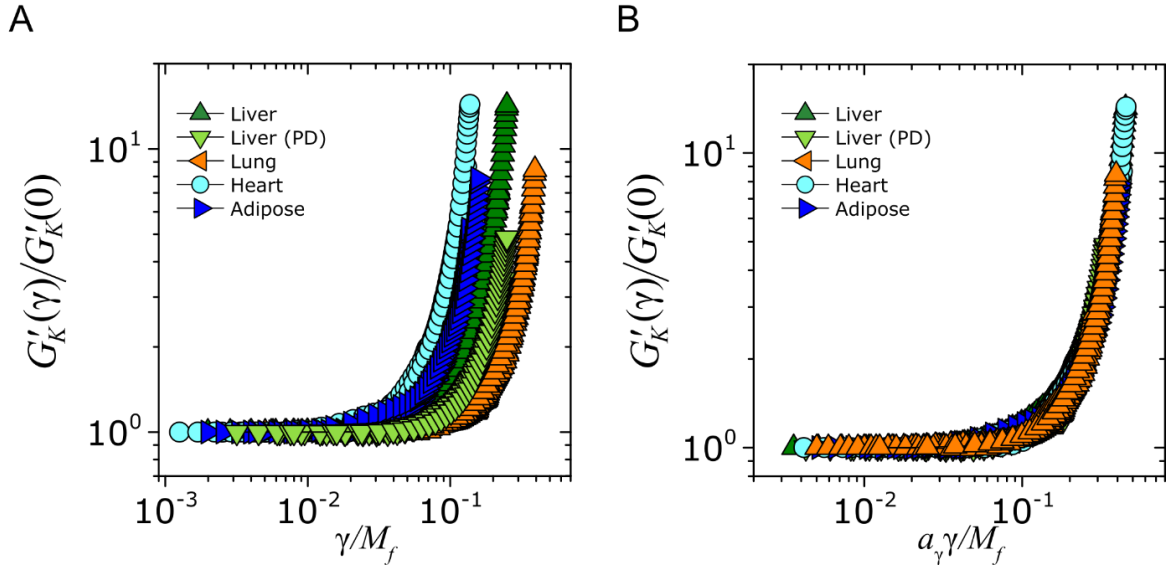


Figure S20. Strain-dependent differential storage modulus $G'_K(\gamma)$ as a function of γ , A) before and B) after shifting with the strain amplification factor a_γ .

Results from repeat experiments on tissues

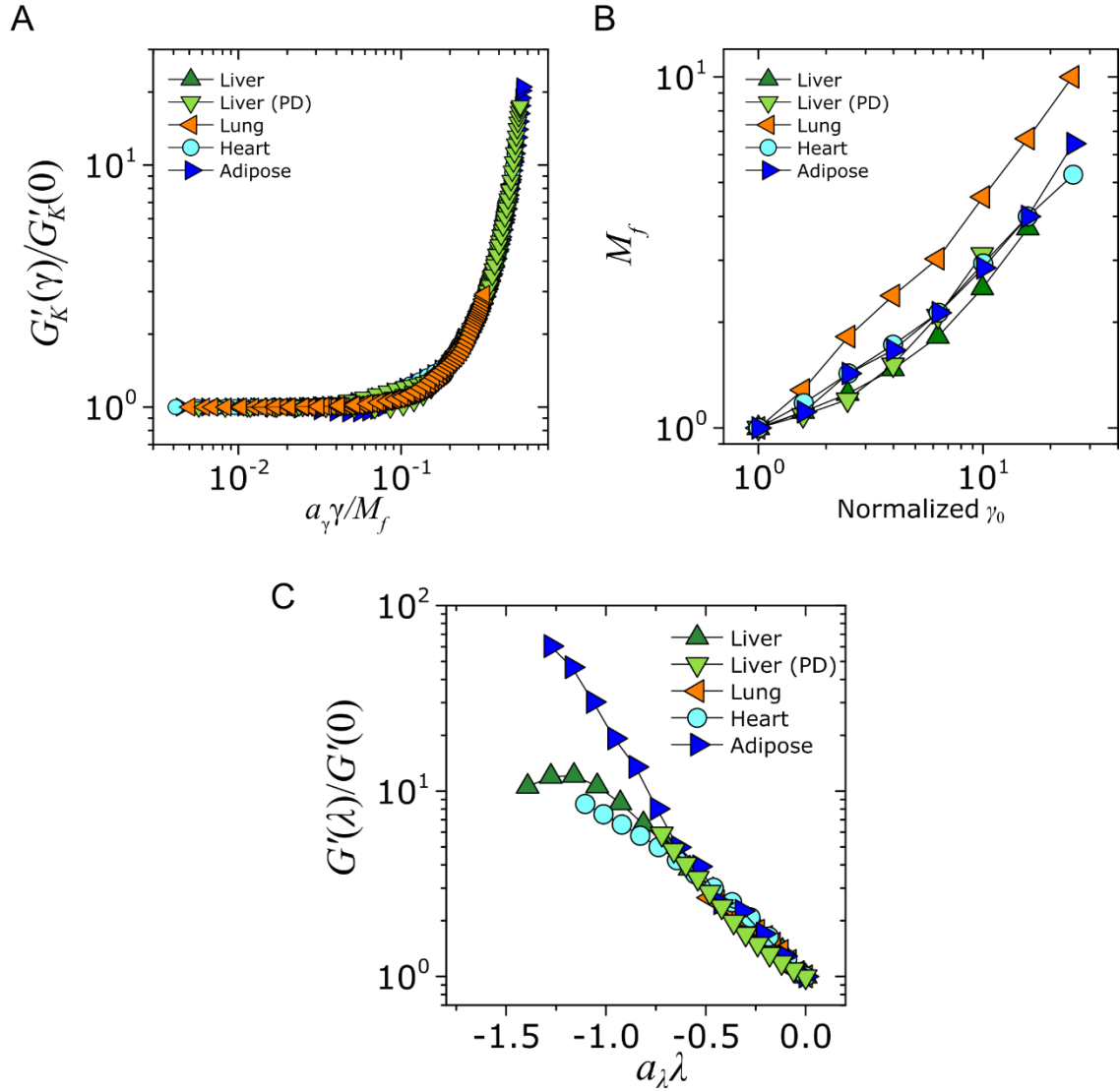


Figure S21. Results from repeats of shear and compression stiffening tests on tissues. A) Shear stiffening master curve, and B) associated Mullins factor M_f from the repeat experiments. C) Compression stiffening master curves. The data shown here are used to obtain statistics for Fig. 3H.

Representative gelation plot of pectin and composite hydrogels

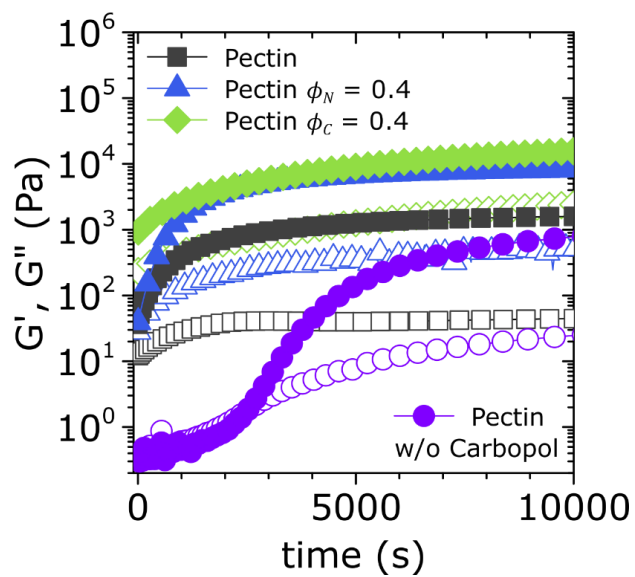


Figure S22. Gelation plot of the pectin hydrogels (with and without Carbopol additives), as well as composite hydrogels with varying ε .

References

- 1 Storm, C., Pastore, J. J., MacKintosh, F., Lubensky, T. & Janmey, P. A. Nonlinear elasticity in biological gels. *Nature* **435**, 191-194 (2005).
- 2 Burla, F., Mulla, Y., Vos, B. E., Aufderhorst-Roberts, A. & Koenderink, G. H. From mechanical resilience to active material properties in biopolymer networks. *Nature Reviews Physics* **1**, 249-263 (2019).
- 3 Van Oosten, A. S. *et al.* Emergence of tissue-like mechanics from fibrous networks confined by close-packed cells. *Nature* **573**, 96-101 (2019).
- 4 Mullins, L. Softening of rubber by deformation. *Rubber Chemistry and Technology* **42**, 339-362 (1969).
- 5 Ewoldt, R. H., Hosoi, A. & McKinley, G. H. New measures for characterizing nonlinear viscoelasticity in large amplitude oscillatory shear. *Journal of Rheology* **52**, 1427-1458 (2008).
- 6 Discher, D. E., Janmey, P. & Wang, Y.-I. Tissue cells feel and respond to the stiffness of their substrate. *Science* **310**, 1139-1143 (2005).
- 7 Kratochvil, M. J. *et al.* Engineered materials for organoid systems. *Nature Reviews Materials* **4**, 606-622, doi:10.1038/s41578-019-0129-9 (2019).
- 8 Kai, F., Drain, A. P. & Weaver, V. M. The extracellular matrix modulates the metastatic journey. *Developmental Cell* **49**, 332-346 (2019).
- 9 Shivers, J. L. *et al.* Compression stiffening of fibrous networks with stiff inclusions. *Proceedings of the National Academy of Sciences* **117**, 21037-21044 (2020).
- 10 Rubinstein, M. & Colby, R. H. *Polymer Physics*. Vol. 23 (Oxford University Press, 2003).
- 11 Song, Y. & Zheng, Q. A guide for hydrodynamic reinforcement effect in nanoparticle-filled polymers. *Critical Reviews in Solid State and Materials Sciences* **41**, 318-346 (2016).
- 12 Smallwood, H. M. Limiting law of the reinforcement of rubber. *Journal of Applied Physics* **15**, 758-766 (1944).
- 13 Guth, E. Theory of filler reinforcement. *Journal Of Applied Physics* **16**, 20-25 (1945).
- 14 Batchelor, G. & Green, J. The determination of the bulk stress in a suspension of spherical particles to order c^2 . *Journal of Fluid Mechanics* **56**, 401-427 (1972).
- 15 Huang, J., Zhou, J. & Liu, M. Interphase in polymer nanocomposites. *JACS Au* **2**, 280-291 (2022).
- 16 Shen, J., Lin, X., Liu, J. & Li, X. Revisiting stress-strain behavior and mechanical reinforcement of polymer nanocomposites from molecular dynamics simulations. *Physical Chemistry Chemical Physics* **22**, 16760-16771 (2020).
- 17 Pogoda, K. *et al.* Compression stiffening of brain and its effect on mechanosensing by glioma cells. *New Journal of Physics* **16**, 075002 (2014).
- 18 Payne, A. R. The dynamic properties of carbon black-loaded natural rubber vulcanizates. Part I. *Journal Of Applied Polymer Science* **6**, 57-63 (1962).
- 19 Hyun, K. *et al.* A review of nonlinear oscillatory shear tests: Analysis and application of large amplitude oscillatory shear (LAOS). *Progress in Polymer Science* **36**, 1697-1753 (2011).
- 20 Ewoldt, R. H., Hosoi, A. E. & McKinley, G. H. Nonlinear viscoelastic biomaterials: meaningful characterization and engineering inspiration. *Integrative and Comparative Biology* **49**, 40-50 (2009).
- 21 Gardel, M. *et al.* Elastic behavior of cross-linked and bundled actin networks. *Science* **304**, 1301-1305 (2004).
- 22 Burla, F., Tauber, J., Dussi, S., van Der Gucht, J. & Koenderink, G. H. Stress management in composite biopolymer networks. *Nature Physics* **15**, 549-553 (2019).
- 23 Donley, G. J., Singh, P. K., Shetty, A. & Rogers, S. A. Elucidating the G' overshoot in soft materials with a yield transition via a time-resolved experimental strain decomposition. *Proceedings of the National Academy of Sciences* **117**, 21945-21952 (2020).
- 24 Papon, A. *et al.* Solid particles in an elastomer matrix: impact of colloid dispersion and polymer mobility modification on the mechanical properties. *Soft Matter* **8**, 4090-4096 (2012).

- 25 Merabia, S., Sotta, P. & Long, D. R. A microscopic model for the reinforcement and the nonlinear behavior of filled elastomers and thermoplastic elastomers (Payne and Mullins effects). *Macromolecules* **41**, 8252-8266 (2008).
- 26 Walls, H., Caines, S. B., Sanchez, A. M. & Khan, S. A. Yield stress and wall slip phenomena in colloidal silica gels. *Journal of Rheology* **47**, 847-868 (2003).
- 27 Wen, Q., Basu, A., Janmey, P. A. & Yodh, A. G. Non-affine deformations in polymer hydrogels. *Soft Matter* **8**, 8039-8049 (2012).
- 28 Shen, T., O'Hern, C. S. & Shattuck, M. Contact percolation transition in athermal particulate systems. *Physical Review E* **85**, 011308 (2012).
- 29 Bueche, F. Molecular basis for the Mullins effect. *Journal of Applied Polymer Science* **4**, 107-114 (1960).
- 30 Mullins, L. & Tobin, N. Stress softening in rubber vulcanizates. Part I. Use of a strain amplification factor to describe the elastic behavior of filler-reinforced vulcanized rubber. *Journal of Applied Polymer Science* **9**, 2993-3009 (1965).
- 31 Bergström, J. S. & Boyce, M. C. Large strain time-dependent behavior of filled elastomers. *Mechanics of Materials* **32**, 627-644 (2000).
- 32 Chen, Q. *et al.* Mechanical reinforcement of polymer nanocomposites from percolation of a nanoparticle network. *ACS Macro Letters* **4**, 398-402 (2015).
- 33 Surve, M., Pryamitsyn, V. & Ganesan, V. Universality in structure and elasticity of polymer-nanoparticle gels. *Physical Review Letters* **96**, 177805 (2006).
- 34 Andrei, D., Briscoe, B., Luckham, P. & Williams, D. in *Modern Aspects of Colloidal Dispersions* 15-24 (Springer, 1998).
- 35 Kuznetsova, T. G., Starodubtseva, M. N., Yegorenkov, N. I., Chizhik, S. A. & Zhdanov, R. I. Atomic force microscopy probing of cell elasticity. *Micron* **38**, 824-833 (2007).
- 36 De Almeida, P. *et al.* Cytoskeletal stiffening in synthetic hydrogels. *Nature Communications* **10**, 609 (2019).
- 37 de Cagny, H. C. *et al.* Porosity governs normal stresses in polymer gels. *Physical Review Letters* **117**, 217802 (2016).
- 38 MacKintosh, F., Käs, J. & Janmey, P. Elasticity of semiflexible biopolymer networks. *Physical Review Letters* **75**, 4425 (1995).
- 39 Bustamante, C., Marko, J. F., Siggia, E. D. & Smith, S. Entropic elasticity of λ -phage DNA. *Science* **265**, 1599-1600 (1994).
- 40 Marszalek, P. E., Li, H., Oberhauser, A. F. & Fernandez, J. M. Chair-boat transitions in single polysaccharide molecules observed with force-ramp AFM. *Proceedings of the National Academy of Sciences* **99**, 4278-4283 (2002).
- 41 Haverkamp, R. G., Marshall, A. T. & Williams, M. Model for stretching elastic biopolymers which exhibit conformational transformations. *Physical Review E* **75**, 021907 (2007).
- 42 Bertula, K. *et al.* Strain-stiffening of agarose gels. *ACS Macro Letters* **8**, 670-675 (2019).
- 43 Liu, Y., Lin, S.-H., Chuang, W.-T., Dai, N.-T. & Hsu, S.-h. Biomimetic strain-stiffening in chitosan self-healing hydrogels. *ACS Applied Materials & Interfaces* **14**, 16032-16046 (2022).
- 44 Liu, X. & Pollack, G. H. Mechanics of F-actin characterized with microfabricated cantilevers. *Biophysical Journal* **83**, 2705-2715 (2002).
- 45 Bozec, L. & Horton, M. Topography and mechanical properties of single molecules of type I collagen using atomic force microscopy. *Biophysical Journal* **88**, 4223-4231 (2005).
- 46 Liu, X., Sun, J. Q., Heggeness, M. H., Yeh, M.-L. & Luo, Z.-P. Force-mediated dissociation of proteoglycan aggregate in articular cartilage. *Biorheology* **43**, 183-190 (2006).
- 47 Lindström, S. B., Kulachenko, A., Jawerth, L. M. & Vader, D. A. Finite-strain, finite-size mechanics of rigidly cross-linked biopolymer networks. *Soft Matter* **9**, 7302-7313 (2013).
- 48 Gutsman, T. *et al.* Force spectroscopy of collagen fibers to investigate their mechanical properties and structural organization. *Biophysical Journal* **86**, 3186-3193 (2004).

- 49 Licup, A. J., Sharma, A. & MacKintosh, F. C. Elastic regimes of subisostatic athermal fiber networks. *Physical Review E* **93**, 012407 (2016).
- 50 Sharma, A. *et al.* Strain-controlled criticality governs the nonlinear mechanics of fibre networks. *Nature Physics* **12**, 584-587 (2016).
- 51 Puxkandl, R. *et al.* Viscoelastic properties of collagen: synchrotron radiation investigations and structural model. *Philosophical Transactions of the Royal Society of London. Series B: Biological Sciences* **357**, 191-197 (2002).
- 52 Webber, R. E., Creton, C., Brown, H. R. & Gong, J. P. Large strain hysteresis and mullins effect of tough double-network hydrogels. *Macromolecules* **40**, 2919-2927 (2007).
- 53 Yuan, H. *et al.* Synthetic fibrous hydrogels as a platform to decipher cell–matrix mechanical interactions. *Proceedings of the National Academy of Sciences* **120**, e2216934120 (2023).
- 54 Hall, M. S. *et al.* Fibrous nonlinear elasticity enables positive mechanical feedback between cells and ECMs. *Proceedings of the National Academy of Sciences* **113**, 14043-14048 (2016).
- 55 Han, Y. L. *et al.* Cell contraction induces long-ranged stress stiffening in the extracellular matrix. *Proceedings of the National Academy of Sciences* **115**, 4075-4080 (2018).
- 56 Frantz, C., Stewart, K. M. & Weaver, V. M. The extracellular matrix at a glance. *Journal of Cell Science* **123**, 4195-4200 (2010).
- 57 Chin, L., Xia, Y., Discher, D. E. & Janmey, P. A. Mechanotransduction in cancer. *Current Opinion in Chemical Engineering* **11**, 77-84 (2016).
- 58 Hashemnejad, S. M. & Kundu, S. Strain stiffening and negative normal stress in alginate hydrogels. *Journal of Polymer Science Part B: Polymer Physics* **54**, 1767-1775 (2016).
- 59 Punter, M. T., Vos, B. E., Mulder, B. M. & Koenderink, G. H. Poroelasticity of (bio) polymer networks during compression: theory and experiment. *Soft Matter* **16**, 1298-1305 (2020).
- 60 Mach, O. & Lacko, L. Density gradient in a dextran medium. *Analytical Biochemistry* **22**, 393-397 (1968).
- 61 Beris, A., Tsamopoulos, J., Armstrong, R. & Brown, R. Creeping motion of a sphere through a Bingham plastic. *Journal of Fluid Mechanics* **158**, 219-244 (1985).
- 62 Xie, Q. *et al.* Astral hydrogels mimic tissue mechanics by aster-aster interpenetration. *Nature Communications* **12**, 4277 (2021).
- 63 Van Oosten, A. S. *et al.* Uncoupling shear and uniaxial elastic moduli of semiflexible biopolymer networks: compression-softening and stretch-stiffening. *Scientific Reports* **6**, 1-9 (2016).
- 64 Pogoda, K. *et al.* Unique Role of Vimentin Networks in Compression Stiffening of Cells and Protection of Nuclei from Compressive Stress. *Nano Letters* (2022).
- 65 Broedersz, C. P. *et al.* Cross-link-governed dynamics of biopolymer networks. *Physical Review Letters* **105**, 238101 (2010).
- 66 Dargazany, R. & Itskov, M. Constitutive modeling of the Mullins effect and cyclic stress softening in filled elastomers. *Physical Review E* **88**, 012602 (2013).